

Nematicity from mixed $S_{\pm} + d_{x^2-y^2}$ states in iron-based superconductors

G. Livanas,¹ A. Aperis,^{1,2} P. Kotetes,³ and G. Varelogiannis¹

¹*Department of Physics, National Technical University of Athens, GR-15780 Athens, Greece*

²*Department of Physics and Astronomy, Uppsala University, Box 516, S-751 20 Uppsala, Sweden*

³*Institut für Theoretische Festkörperphysik, Karlsruhe Institute of Technology, D-76128 Karlsruhe, Germany*

(Received 14 June 2013; revised manuscript received 23 January 2015; published 2 March 2015)

We propose a novel mechanism for nematicity potentially relevant in some iron-based superconductors (SCs). We demonstrate that the mixed $S_{\pm} + d_{x^2-y^2}$ SC state is a physically accessible state and may emerge under generic conditions, lowering spontaneously the fourfold rotational symmetry C_4 to C_2 . We provide a detailed study of the mixed $S_{\pm} + d_{x^2-y^2}$ nematic state including its behavior under a Zeeman field. As a fingerprint of this state, we predict at low temperatures a first-order Zeeman-field-induced transition from the mixed nematic SC phase to the pure $d_{x^2-y^2}$ SC phase. The Zeeman field–temperature phase diagram for a nodeless mixed nematic state exhibits three distinct SC phases and a tetracritical point, remarkably reminiscent of the one observed in $U\text{Pt}_3$. Our mechanism for nematicity may also be relevant for nonsuperconducting nematic states involving mixed $S_{\pm} + d_{x^2-y^2}$ spin/charge density waves.

DOI: [10.1103/PhysRevB.91.104502](https://doi.org/10.1103/PhysRevB.91.104502)

PACS number(s): 71.27.+a, 74.20.Rp, 74.70.Xa

I. INTRODUCTION

In iron-based superconductors (SCs), fundamental aspects concerning the SC gap structure still remain controversial. In a series of materials such as $\text{Ba}_{1-x}\text{K}_x\text{Fe}_2\text{As}_2$, $\text{BaFe}_{2-x}\text{Co}_x\text{As}_2$, $\text{FeTe}_{1-x}\text{Se}_x$, and $\text{K}_x\text{Fe}_{2-x}\text{Se}_2$ there is experimental evidence for nodeless SCs [1]. Apparently, this is not the conventional isotropic s -wave gap but, instead, the extended S_{\pm} gap changing sign between the electron and hole pockets of the Fermi surface (FS) [2]. On the other hand, in materials such as KFe_2As_2 , LiFeP , LaOFeP , $\text{BaFe}(\text{As}_{1-x}\text{P}_x)_2$, and $\text{BaFe}_{2-x}\text{Ru}_x\text{As}_2$, diverse experiments including NMR, STM, thermal conductivity, and penetration depth measurements all point to the presence of gap nodes on the FS [3].

The above experiments advocate that iron-based SCs are a family of materials that exhibit a pronounced fragility of the gap symmetry. In fact, recent works have demonstrated the possibility of gap symmetry transitions [4–8], independently of the pairing mechanism. Although the spin-fluctuations scenario [6–8] and the small- q electron-phonon interaction (EPI) [4,5] are both compatible, gap symmetry transitions constitute a characteristic feature of the latter mechanism, since it naturally leads to a loss of rigidity of the gap function in momentum space, a property called momentum decoupling [9]. Note that small- q EPI can produce nodeless S_{\pm} as well as nodal SC states depending on doping [4], including chiral triplet p -wave SC [5], observed recently in LiFeAs [10]. Moreover, recent ARPES results on FeSe films deposited on SrTiO_3 provide evidence for the relevance of small- q phonon processes [11].

Apart from the unclear SC gap symmetry, recent STM measurements on FeSe revealed another puzzling feature of iron-based SCs. Iron selenide has been considered as one of the simplest iron-based SCs [12,13] with most probably EPI-mediated SC [14] and $T_c \sim 9$ K. Tunneling conductance measurements by Song *et al.* [15] on crystalline FeSe films report sharp evidence for nematicity. Nematicity in iron pnictides is a highly debated issue, following numerous reports for a possible electronic nematic phase transition [16,17] that often coincides and possibly drives the orthorhombic distortion [18–20] which sometimes accompanies an antiferromagnetic

(AFM) transition in undoped and underdoped compounds. Because of the near coincidence of nematicity and AFM in some compounds, it has been suggested that the magnetism itself may drive an electronic nematic phase transition [21–24].

However, in other compounds such as in the case of FeSe , there are no such AFM phases involved [25]. The AFM-independent orbital ordering scenario [26,27] has been invoked recently [28] for interpreting the nematic findings in SC FeSe films. In fact, a tiny orthorhombic distortion has been observed by synchrotron x-ray power diffraction at about 90 K in FeSe [25], which according to other experiments may indicate orbital ordering [29], in which case the orthorhombic character of the electronic system is enhanced and this could explain in that case nematic SC. It is unclear whether the observed nematic SC phase is nodal or nodeless. The STM experiments that reported nematicity have also explicitly revealed the existence of line nodes in the nematic SC gap function [15], in agreement with previous NMR data [30]. These findings however contradict thermal conductivity [31] and specific-heat [32] measurements that indicate a nodeless SC gap.

Here we put forward an approach to the phenomenon of nematicity that may be relevant in some iron-based SCs in which strong nematicity is not evident in the normal state. Motivated by their tendency towards gap symmetry transitions, we demonstrate (Fig. 1) that the S_{\pm} and $d_{x^2-y^2}$ gap symmetries may broadly coexist and the resulting mixed $S_{\pm} + d_{x^2-y^2}$ SC is a prominent nematic phase that may emerge spontaneously in some of these materials. Note that this is not the global minimum of the free energy within our mean-field approach. In fact, the T -breaking $S_{\pm} + id$ tetragonal mixed state has a slightly lower free energy. However, it is nearly degenerate with the mixed $S_{\pm} + d$ nematic state and additional phenomena such as nematic fluctuations [33], spontaneous edge currents in a finite sample of a T -breaking mixed state [34], and induced nematicity phenomena may all contribute to lift the degeneracy in favor of the mixed nematic state.

Depending on the relative strength of the gap in each contributing symmetry channel of our mixed nematic state, the resulting nematic SC can be either nodal or nodeless.

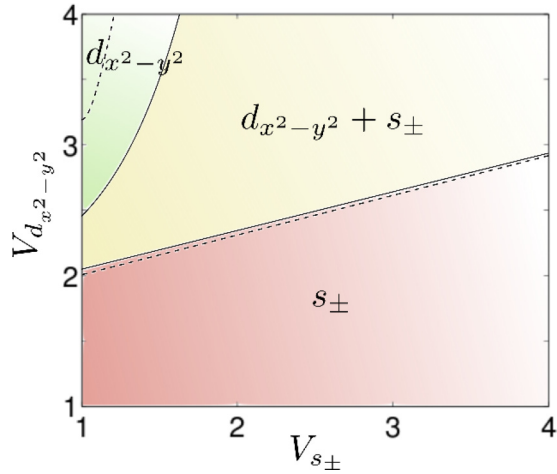


FIG. 1. (Color online) Landscape of the possible SC phases obtained by varying the effective interaction potentials of S_{\pm} and $d_{x^2-y^2}$ from t to $4t$, at $T = 0$. Solid line boundaries correspond to $\mu = 0.05$ and dashed line boundaries to $\mu = 0.4$. We find three distinct regions S_{\pm} , $S_{\pm} + d_{x^2-y^2}$, and $d_{x^2-y^2}$. Notice the extended region over which S_{\pm} and $d_{x^2-y^2}$ coexist leading to a nematic SC phase. The nematic region expands with electron doping in expense to the pure $d_{x^2-y^2}$ region while the pure S_{\pm} region remains essentially the same.

Within a minimal two-band model, we show that at low temperatures a Zeeman field can induce a first-order transition from the nematic $S_{\pm} + d_{x^2-y^2}$ phase to the pure $d_{x^2-y^2}$ phase. We therefore propose an experimental strategy for confirming the eventual presence of mixed $S_{\pm} + d_{x^2-y^2}$ states in films by applying an in-plane magnetic field in which case the Zeeman effects will dominate [35]. Remarkably, our self-consistent study for a nodeless $S_{\pm} + d_{x^2-y^2}$ phase provides a Zeeman field–temperature phase diagram which exhibits three distinct SC regions and a tetracritical point in complete analogy to the situation encountered in UPt₃ [36]. This type of phase diagram is thus reproduced self-consistently within a microscopic two-band picture.

II. THE MODEL

For our general discussion, we qualitatively model iron-based SCs with a minimal two-band model exhibiting a hole pocket around the $\Gamma(0,0)$ point and an electron pocket around the $M(\pi,\pi)$ point, described by the energy dispersions $\varepsilon_e(\mathbf{k}) = \gamma(\mathbf{k}) + \delta(\mathbf{k}) - \mu$ and $\varepsilon_h(\mathbf{k}) = \gamma(\mathbf{k}) - \delta(\mathbf{k}) - \mu$, respectively, where we introduce the nearest-neighbor hopping $\gamma(\mathbf{k}) = t(\cos k_x + \cos k_y)$, the next-nearest-neighbor hopping $\delta(\mathbf{k}) = C - t' \cos k_x \cos k_y$, and the chemical potential μ . We also set $t = 1$, $t' = 0.5$, $C = 2$. Notice that since we are working in the folded Brillouin zone (FBZ) with two Fe atoms per cell, each band must preserve C_4 symmetry separately in contrast to previously proposed band models [24,37] defined in the extended BZ. In spite of this difference, the present model captures the necessary FS characteristics allowing for the S_{\pm} state to emerge, namely well separated electron and hole FS sheets. As a matter of fact, the general concept of nematicity driven by mixed SC gap symmetries, proposed here,

will be still valid even if we consider other sophisticated band structure models [38]. Even more, to keep our analysis also independent of the detailed pairing mechanism, we consider a separable effective interaction, allowing for a broad discussion concerning a large number of compounds.

Under the aforementioned assumptions we have

$$\mathcal{H} = \sum_{\mathbf{k},\sigma} [\varepsilon_e(\mathbf{k})c_{\mathbf{k},\sigma}^\dagger c_{\mathbf{k},\sigma} + \varepsilon_h(\mathbf{k})d_{\mathbf{k},\sigma}^\dagger d_{\mathbf{k},\sigma}] - \frac{1}{N} \sum_{\mathbf{k},\mathbf{k}'} V(\mathbf{k},\mathbf{k}') \widehat{\mathcal{D}}_{\mathbf{k}}^\dagger \widehat{\mathcal{D}}_{\mathbf{k}'}, \quad (1)$$

where $c_{\mathbf{k},\sigma}^{(\dagger)}$ and $d_{\mathbf{k},\sigma}^{(\dagger)}$ are annihilation (creation) operators for the electron $\varepsilon_e(\mathbf{k})$ and hole $\varepsilon_h(\mathbf{k})$ bands, respectively, of spin projection $\sigma = \uparrow, \downarrow$, while N denotes the number of lattice points. We also introduced the pairing operator $\widehat{\mathcal{D}}_{\mathbf{k}} \equiv c_{-\mathbf{k},\downarrow} c_{\mathbf{k},\uparrow} + d_{-\mathbf{k},\downarrow} d_{\mathbf{k},\uparrow}$. Notice that for the specific choice of the interaction, where intraband and interband strengths are equal, electron and hole bands share the same SC order parameter $\Delta(\mathbf{k})$, which is defined in the following manner:

$$\Delta(\mathbf{k}) = -\frac{1}{N} \sum_{\mathbf{k}'} V(\mathbf{k},\mathbf{k}') \langle \widehat{\mathcal{D}}_{\mathbf{k}'} \rangle. \quad (2)$$

The order parameter $\Delta(\mathbf{k}) = \sum_n \Delta_n f_n(\mathbf{k})$ consists of irreducible representations (IRs) $f_n(\mathbf{k})$ of the relevant point group for the non-SC tetragonal phase, which is D_{4h} for bulk systems and C_{4v} for films, that both include C_4 as a subgroup. Here we shall restrict our analysis to the following on-site and nearest-neighbor IRs: $f_s(\mathbf{k}) = 1$ (A_1), $f_{s_{\pm}}(\mathbf{k}) = \cos k_x + \cos k_y$ (A_1), and $f_a(\mathbf{k}) = \cos k_x - \cos k_y$ (B_1). By studying here the SC phase competition via separable potentials we report generic results that are broadly relevant, and independent of the exact microscopic mechanism of SC.

Within the aforementioned subspace of IRs, there are only two minimal schemes to achieve a nematic state. These are the mixed states $S + d_{x^2-y^2}$ and $S_{\pm} + d_{x^2-y^2}$. Of course, the cases $S + S_{\pm} + d_{x^2-y^2}$, $iS + S_{\pm} + d_{x^2-y^2}$, $S + iS_{\pm} + d_{x^2-y^2}$ are also possible but not minimal. In all these symmetry-breaking patterns the subgroup C_4 reduces to C_2 . Notice that for a minimal nematic phase, the two IRs involved must lock in the same phase. If the two phases lock in phases with $\pi/2$ difference then the mixed state leads to broken \mathcal{T} but unbroken C_4 . These states are also important and for completeness we shall also discuss features of their phase diagram and their phenomenology (see also [33,39]).

We consider first the minimal configurations in which nematicity emerges and \mathcal{T} is preserved. In these cases the order parameter $\Delta(\mathbf{k})$ is the sum of two order parameters $\Delta_{1,2}(\mathbf{k})$ corresponding to the two coexisting IRs. For simplicity we shall consider that $\Delta_{1,2}(\mathbf{k})$ are real. At this point, we introduce the spinor $\Psi_{\mathbf{k}}^\dagger = (c_{\mathbf{k},\uparrow}^\dagger, d_{\mathbf{k},\uparrow}^\dagger, c_{-\mathbf{k},\downarrow}^\dagger, d_{-\mathbf{k},\downarrow}^\dagger)$ and employ the $\boldsymbol{\tau}$ and $\boldsymbol{\rho}$ Pauli matrices acting on particle-hole and band spaces, respectively. The mean-field Hamiltonian can be rewritten compactly as $\mathcal{H} = \sum_{\mathbf{k}} \widehat{\Psi}_{\mathbf{k}}^\dagger \widehat{\mathcal{H}}(\mathbf{k}) \widehat{\Psi}_{\mathbf{k}}$ with

$$\widehat{\mathcal{H}}(\mathbf{k}) = [\gamma(\mathbf{k}) - \mu] \hat{\tau}_3 + \delta(\mathbf{k}) \hat{\tau}_3 \hat{\rho}_3 + \Delta(\mathbf{k}) \hat{\tau}_1 - \mathcal{B}, \quad (3)$$

where we also incorporated the effect of a Zeeman field \mathcal{B} . With the usual techniques we calculate the corresponding Matsubara

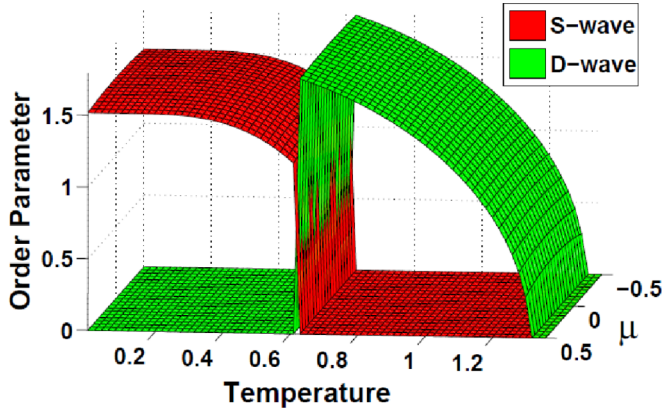


FIG. 2. (Color online) Typical temperature-induced first-order transition from S (red) to $d_{x^2-y^2}$ SC (green) for various chemical potentials μ obtained when $V_S < V_{d_{x^2-y^2}} < 1.5V_S$. Free energy calculations not reported here confirm this transition. A mixed $S + d_{x^2-y^2}$ state is not accessible.

Green's function, which exhibits four quasiparticle branches, and then solve the coupled self-consistent equations, which provide the two gaps $\Delta_{1,2}(\mathbf{k})$.

III. THE MAIN RESULTS

To illustrate the fact that achieving mixed states is not a trivial task, we start with the competition between the isotropic S IR and the $d_{x^2-y^2}$ IR. As expected, S and $d_{x^2-y^2}$ SC phases are highly competitive and coexistence cannot be achieved at any value of the respective potentials. Remarkably, when $V_S < V_{d_{x^2-y^2}} < 1.5V_S$ we observe a first-order transition from $d_{x^2-y^2}$ to S gap symmetry as we lower the temperature (Fig. 2). We confirmed the validity of this transition by verifying that it constitutes a global minimum solution of the free energy calculated as described in Appendix A.

While the isotropic S SC phase cannot coexist with the $d_{x^2-y^2}$ SC phase, the S_{\pm} phase that is widely considered relevant for iron-based SCs coexists with $d_{x^2-y^2}$ over a wide range of the effective potentials (Fig. 1). The reason for this different behavior is deeply rooted in the nonisotropic momentum structure of the S_{\pm} IR. In Fig. 3 we report typical self-consistent solutions of the SC gap function in the mixed nematic $S_{\pm} + d_{x^2-y^2}$ SC phase in the case of nodal [Fig. 3(a)] and nodeless [Fig. 3(b)] SC gaps. We insist that all the effective potentials and dispersions used in our self-consistent calculations preserve C_4 symmetry. Only because S_{\pm} and $d_{x^2-y^2}$ coexist, fourfold rotational symmetry is spontaneously broken and nematicity emerges. The essential ingredients leading to the nematic $S_{\pm} + d_{x^2-y^2}$ state is on one hand the well separated electron and hole pockets that favor the stabilization of the S_{\pm} phase and on the other, some weak tendency towards the formation of the $d_{x^2-y^2}$ gap symmetry that is not suppressed by the presence of S_{\pm} .

The detailed characteristics of the FS topology are not crucial for the formation of the nematic state but mainly determine, along with the exact ratio of the S_{\pm} and $d_{x^2-y^2}$ order parameters, the nodal or nodeless type of the quasiparticle excitation spectrum (this is detailed in Appendix B). Depending on

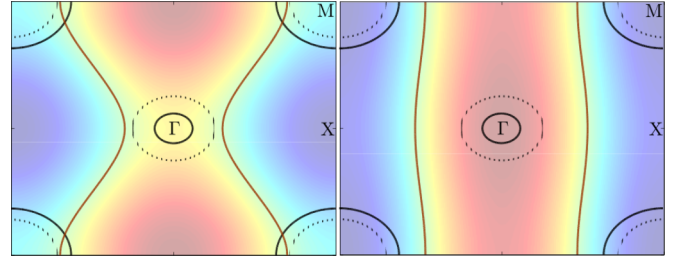


FIG. 3. (Color online) The self-consistently obtained total SC gap amplitude in the nematic $S_{\pm} + d_{x^2-y^2}$ phase for the case when (a) the dominating component is the $d_{x^2-y^2}$ and (b) the S_{\pm} . The color grade shows the momentum structure of the gap over the whole FBZ [red (blue) is for positive (negative) values]. The magenta lines denote the area where the SC gap vanishes, i.e., the SC gap nodes. In the same plots is shown the FS for two cases of electron doping $\mu = (0.05, 0.4)$, drawn with dotted and solid lines, respectively. Note that for both dopings the SC gap structure remains unaltered. (a) Dominating $d_{x^2-y^2}$ component. In this case the nematic SC state can be either nodal or nodeless depending on the doping level. (b) Dominating S_{\pm} component. In this case the nematic SC state can only be nodeless. Note that in both cases the fourfold rotational C_4 symmetry is reduced to C_2 .

the nature of the spectrum a peculiar quantum critical behavior can emerge [40]. Even more, a nodal nematic $S_{\pm} + d_{x^2-y^2}$ SC phase, which was self-consistently obtained within the small- q phonon pairing mechanism, was also reported in Figs. 2(f) and 4(d) of Ref. [4]. A recent spin-fluctuations model also appears compatible [33]. These small- q results confirm that the present findings of the separable potentials analysis are generic. The occurrence of the nematic $S_{\pm} + d_{x^2-y^2}$ SC phase is indeed a detail-independent phenomenon, not requiring fine-tuning on a particular microscopic model.

More importantly, the distinctive behavior of the mixed $S_{\pm} + d_{x^2-y^2}$ state in the presence of a Zeeman field may provide additional routes for its experimental identification. At low temperatures, we obtain a characteristic first-order field-induced transition from the nematic $S_{\pm} + d_{x^2-y^2}$ phase to the pure $d_{x^2-y^2}$ phase (Fig. 4). The transition exists only at sufficiently low temperatures. By exploring the higher temperature regime in the presence of the field, we construct the self-consistent Zeeman field-temperature phase diagram. Quite remarkably, for the $T = B = 0$ nodeless nematic solution shown in Fig. 3, we obtain a B - T phase diagram exhibiting three distinct SC regions and a tetracritical point [Fig. 4(a)]. The latter is analogous to the well known phase diagram of UPt₃, obtained also in the presence of in-plane fields [36].

In our case this phase diagram can be understood as follows: the S_{\pm} gap symmetry is dominant for the particular case, owing the higher T_c at zero field. On the other hand, in the presence of a large Zeeman field, the $d_{x^2-y^2}$ gap symmetry with nodes on the FS is energetically more favorable than a nodeless SC phase [41] and thus the nodal gap exhibits a higher critical field at zero temperature. Therefore, the reason for such a complicated phase diagram lies in the extraordinary fact that at zero field, a fully gapped SC phase like S_{\pm} allows at lower temperatures its coexistence with an emergent nodal $d_{x^2-y^2}$ phase. This phase diagram occurs only for fully gapped nematic phases at zero field. In the case when the $T = B = 0$ nematic solution is

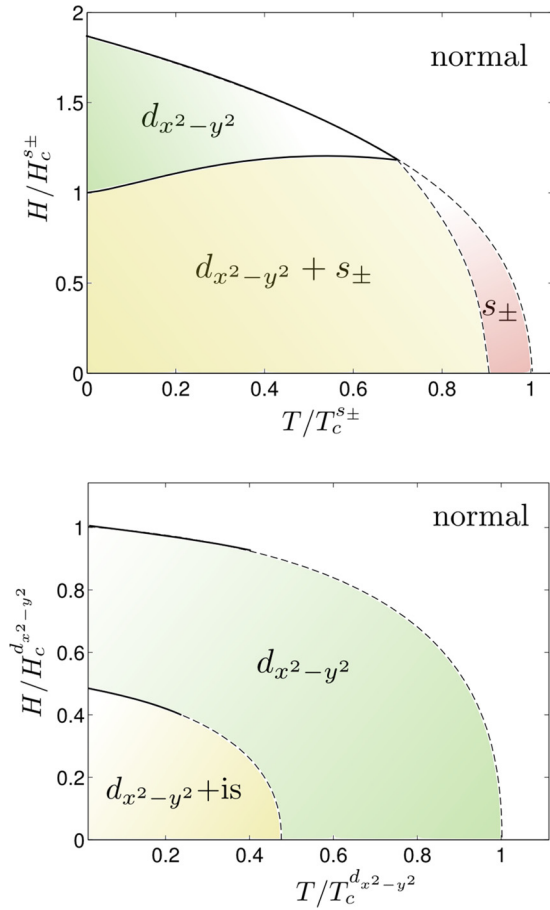


FIG. 4. (Color online) Zeeman field–temperature phase diagrams resulting from our self-consistent calculations for $\mu = 0.4$. Solid (dashed) lines denote first (second) order phase transitions. (a) Case shown in Fig. 3(b). It exhibits three distinct superconducting regions and a tetracritical point. A similar diagram has been experimentally observed in UPt_3 [36]. (b) Case of mixed $S + id_{x^2-y^2}$ states that break time-reversal invariance but preserve the tetragonal symmetry. Note that in both cases there is a low-temperature first-order transition from mixed to pure $d_{x^2-y^2}$ SC states as the field increases.

nodal, the phase diagram has the same qualitative form as in Fig. 4(b). In both cases, an experimental method for identifying the mixed character of the proposed $S_{\pm} + d_{x^2-y^2}$ nematic SC phase is the observation of a Zeeman-field-induced first-order transition from the mixed nematic $S_{\pm} + d_{x^2-y^2}$ state to the pure $d_{x^2-y^2}$ state that is nodal and preserves C_4 .

Mixed states may also lead to \mathcal{T} breaking, if the coexisting order parameters lock in a $\pi/2$ phase difference. In that case C_4 symmetry is preserved, rendering the \mathcal{T} -breaking $S_{\pm} + id_{x^2-y^2}$ mixed phases clearly distinguishable from the nematic $S_{\pm} + d_{x^2-y^2}$ in experiments sensitive to the in-plane anisotropy. Within our mean-field approach the \mathcal{T} -breaking $S_{\pm} + id_{x^2-y^2}$ phase has slightly lower free energy than the nematic $S_{\pm} + d_{x^2-y^2}$ state. However, from our systematic numerical exploration we conclude that this difference may be so small that the $S_{\pm} + d_{x^2-y^2}$ and $S_{\pm} + id_{x^2-y^2}$ mixed states may be regarded as nearly degenerate (see Appendix A). Note that the phase diagram related to the $S_{\pm} + id_{x^2-y^2}$ SC phase exhibits no qualitative difference compared to the previously presented

phase diagrams for the nematic $S_{\pm} + d_{x^2-y^2}$. Moreover, the presence of induced electronic nematicity phenomena and nematic fluctuations [33] contributes to stabilize the nematic SC phase. This is substantiated in Appendix C. In addition, the states that break \mathcal{T} are disfavored by spontaneous currents and other mesoscopic phenomena [34] that we will not treat here.

On the other hand, the \mathcal{T} -violating $S + id_{x^2-y^2}$ SC phase is always characterized by a phase diagram as in Fig. 4(b) and can never exhibit a tetracritical point, because according to our self-consistent calculations and in agreement with prior studies [42], the mixed $S + id_{x^2-y^2}$ phase only appears for sufficiently large $d_{x^2-y^2}$ potentials $V_{d_{x^2-y^2}} > 1.2V_S$. Therefore, the nodal $d_{x^2-y^2}$ phase with the higher critical field owes at the same time the higher T_c at zero field. Note that here as well we obtain at low T a first-order Zeeman-field-induced transition from the mixed $S + id_{x^2-y^2}$ phase to the pure $d_{x^2-y^2}$ phase.

IV. DISCUSSION AND CONCLUSION

A mechanism for nematicity is demonstrated here. Our results indicate that the mixed nematic SC state $S_{\pm} + d_{x^2-y^2}$ may be accessible under generic conditions within our two-band mean-field model. Similar results can be obtained if we include the next-nearest-neighbor IRs: $f_s(\mathbf{k}) = 2 \cos k_x \cos k_y$ (A_1) and $f_d(\mathbf{k}) = 2 \sin k_x \sin k_y$ (B_2) (see Appendix D). Moreover our mechanism is not restricted to nematic superconducting phases. Our findings can be directly extrapolated to unconventional density wave (DW) phases as well. In fact, when the two bands are perfectly nested, our results for the interplay of S_{\pm} and $d_{x^2-y^2}$ SCs hold identically for the corresponding interband $S_{\pm} + d_{x^2-y^2}$ spin density wave (SDW) case, based on the mapping $\mathcal{B}_{sc} \rightarrow \mu_{sdw}$. This is illustrated in Appendix E. Moreover, in the particle-hole asymmetric case the situation changes, with the basic feature being that a spin DW and a charge DW exhibiting the same momentum structure are coupled in the presence of a Zeeman field [43] because they form a quartet [44]. Note that a spontaneously emerging mixed nematic charge DW may as well drive an orthorhombic distortion to the lattice in the form of a Peierls instability.

An eventual identification of some iron-based materials in which our mechanism may be the origin of nematicity in a SDW phase would have serious implications even about the nature of the eventual nonnematic SDW phases. In fact, since the $S + d_{x^2-y^2}$ SDW state is not accessible, if the mixed nematic SDW state $S_{\pm} + d_{x^2-y^2}$ is responsible for nematicity in the AFM phase then we may indirectly conclude that nonnematic AFM phases are most likely of S_{\pm} type and not S type as is usually assumed. In fact in both S and S_{\pm} symmetry channels for an interband SDW we deal with a nodeless real SDW order parameter of the same wave vector and it is almost impossible to distinguish between them directly from experiments. However, these are two different states: S is a conventional and S_{\pm} an unconventional SDW state, which behave differently for example in the proximity of a d -wave condensate. In particular, modeling of coexisting SDW and SC states should treat the SDW phase in the S_{\pm} channel and not in the usual S channel and this will affect the results.

If indeed unconventional SCs in an iron-based compound lie in the proximity of unconventional DW phases of the same order parameter symmetry, then a fundamental analogy to

high- T_c cuprates emerges, where there are reports of a d -wave DW (orbital AFM) phase associated with the pseudogap [45]. In the d -wave DW phase, the orbital coupling to an externally applied magnetic field [46] induces a chiral d -density wave phase [47], which can account for the anomalous Nernst signal [48] observed in the pseudogap phase of cuprates [49]. Note that such anomalies in the Nernst signal are apparently present also in some underdoped iron-pnictides, as well as at temperatures where nematicity emerges [50], leaving the possibility of a chiral mixed nematic spin DW open. We should finally note here that to an unconventional charge density wave particle-hole condensate in momentum space corresponds effectively in the strong-coupling limit an orbital ordering state in real space, exactly as Bose condensation of polarons corresponds to the strong-coupling limit of BCS pairing or localized ferromagnetism corresponds to the strong-coupling limit of a Stoner ferromagnet. Therefore our picture is not totally incompatible with those involving orbital ordering for the nonsuperconducting states. However, additional dedicated work is needed in order to identify firmly mixed nematic SC or DW phases in some iron-based materials, and the search for the low- T Zeeman-field-induced first-order transition from the mixed nematic state to the d -wave tetragonal state may represent a useful approach. To make the link between our microscopic approach and the Landau approach adopted by many authors for related studies, we provide in Appendix F a detailed Landau expansion of our microscopic free energy translating some of our findings in that framework as well.

In conclusion, we introduce a mechanism for nematicity in the SC state and potentially in the antiferromagnetic/charge-ordered state. It consists of the spontaneous emergence of mixed $d_{x^2-y^2} + S_{\pm}$ symmetries in the corresponding SC or DW order parameters. We predict an in-plane field-induced melting of nematicity in films exhibiting such mixed states, via an abrupt first-order transition at low temperatures, to a nodal $d_{x^2-y^2}$ phase preserving C_4 . This transition can be regarded as the fingerprint of the presence of a mixed state. Note that these mixed SC-DW states have a quartet coupling with electronic nematic or Pomeranchuk phases [44] that can therefore be induced stabilizing the mixed nematic SC state (Appendix C). Finally, mixed SC states that break time-reversal symmetry but preserve C_4 are also accessible and should be taken into consideration in the analysis of experiments. Those \mathcal{T} -breaking states are very rare in nature and precious because they may eventually constitute an element for engineering, with a proper choice of proximity effects in nanostructures, relevant topological states. The near degeneracy of our mixed nematic states with the mixed \mathcal{T} -breaking states makes any materials in which our mixed nematic states are eventually observed potentially relevant platforms for engineering the corresponding SC \mathcal{T} -breaking states in properly designed nanostructures. We will examine this possibility in a future work.

ACKNOWLEDGMENTS

We are grateful to Sergey Borisenko, Anna Böhmer, Christoph Meingast, and Jörg Schmalian for illuminating comments on the phenomenology of the pnictides. We acknowledge funding from the PIEBE program of NTUA.

APPENDIX A: FREE ENERGY CALCULATIONS

Defining the spinor $\Psi_{\mathbf{k}}^{\dagger} = (c_{\mathbf{k},\uparrow}^{\dagger}, d_{\mathbf{k},\uparrow}^{\dagger}, c_{-\mathbf{k},\downarrow}, d_{-\mathbf{k},\downarrow})$ we take the Hamiltonian

$$\mathcal{H} = \sum_{\mathbf{k}} \Psi_{\mathbf{k}}^{\dagger} \{ \gamma_{\mathbf{k}} \hat{\tau}_3 \hat{\rho}_0 + \delta_{\mathbf{k}} \hat{\tau}_3 \hat{\rho}_3 - \mu \hat{\tau}_3 \hat{\rho}_0 - \mathcal{B} \hat{\tau}_0 \hat{\rho}_0 + \Delta_1(\mathbf{k}) \hat{\tau}_1 \hat{\rho}_0 + \Delta_2(\mathbf{k}) \hat{\tau}_1 \hat{\rho}_0 \} \Psi_{\mathbf{k}}, \quad (\text{A1})$$

and the corresponding Green's function reads

$$\hat{G}(\mathbf{k}, i\omega_n) = (i\omega_n - \gamma_{\mathbf{k}} \hat{\tau}_3 \hat{\rho}_0 - \delta_{\mathbf{k}} \hat{\tau}_3 \hat{\rho}_3 + \mu \hat{\tau}_3 \hat{\rho}_0 + \mathcal{B} \hat{\tau}_0 \hat{\rho}_0 - \Delta_1(\mathbf{k}) \hat{\tau}_1 \hat{\rho}_0 - \Delta_2(\mathbf{k}) \hat{\tau}_1 \hat{\rho}_0)^{-1}$$

with the poles at $E_{\pm\pm}^{\mathcal{B}}(\mathbf{k}) = -\mathcal{B} \pm E_{\pm}(\mathbf{k})$ with $E_{\pm}(\mathbf{k}) = \sqrt{[\gamma_{\mathbf{k}} \pm \delta_{\mathbf{k}} - \mu]^2 + [\Delta_1(\mathbf{k}) + \Delta_2(\mathbf{k})]^2}$. The free Green's function is just $\hat{G}_0(\mathbf{k}, i\omega_n) = (i\omega_n - \gamma_{\mathbf{k}} \hat{\tau}_3 \hat{\rho}_0 - \delta_{\mathbf{k}} \hat{\tau}_3 \hat{\rho}_3 + \mu \hat{\tau}_3 \hat{\rho}_0 + \mathcal{B} \hat{\tau}_0 \hat{\rho}_0)^{-1}$ and the self-consistent equation for the $\Delta_{1(2)}(\mathbf{k})$ SC order parameters is $\Delta_{1(2)}(\mathbf{k}) = \frac{1}{4} T \sum_{\mathbf{k}', n} V_{\mathbf{k}\mathbf{k}'}^{1(2)} \text{Tr} \{ \hat{\tau}_1 \hat{G}(\mathbf{k}', i\omega_n) \}$. The free energy difference between the condensed and the normal system with the above Hamiltonian can be obtained via the Feynman-Hellmann theorem as

$$\delta\mathcal{F} = \frac{\Delta_1^2}{V_1} + \frac{\Delta_2^2}{V_2} - \frac{1}{2} T \sum_n \sum_{\mathbf{k}'} \text{Tr} \left\{ \ln \frac{\hat{G}^{-1}(\mathbf{k}', i\omega_n)}{\hat{G}_0^{-1}(\mathbf{k}', i\omega_n)} \right\}. \quad (\text{A2})$$

This provides the exact free energy at all temperatures within our approach. In the left panel of Fig. 5 we show as an example the free energy shape that results from our self-consistent calculations in the low- T and zero-field regime of Fig. 4(a) where the physical ground state is the mixed nematic $S_{\pm} + d_{x^2-y^2}$ phase.

As we mention in the main text, the \mathcal{T} -violating phases are also accessible over a wide range of potentials and they may even appear very marginally favored compared to the nematic phase. We report here the results of systematic numerical calculations of both condensation free energies and we conclude that the \mathcal{T} -violating and nematic phases are nearly degenerate especially for the range of potentials $V_d \leq 2.5$ and $V_{s_{\pm}} \leq 2$ (in units of $t = 1$). Indeed, even for $T = 0$ where the relative difference takes maximal values, one can see that this relative difference is nevertheless negligible, lower than 0.3% for potentials $V_d \leq 2.5$ and $V_{s_{\pm}} \leq 2$ [Figs. 5(b) and 5(c)].

This near degeneracy is lifted in favor of the nematic phase by phenomena not taken into consideration here. Such important phenomena are the following:

(1) The unavoidable emergence of spontaneous currents in finite samples with \mathcal{T} -violating condensates will renormalize these condensates. In the nematic phase instead, these phenomena are absent.

(2) Nematic superconductivity induces electronic nematicity phenomena that are cooperative, contributing to stabilize the nematic superconducting phase.

The study of the influence of spontaneous currents in finite samples of \mathcal{T} -violating superconductors is beyond the possibilities of the present approach and will be explored elsewhere. On the other hand, in Appendix C is illustrated how induced Pomeranchuk or electron nematicity phenomena cooperate with nematic superconductivity.

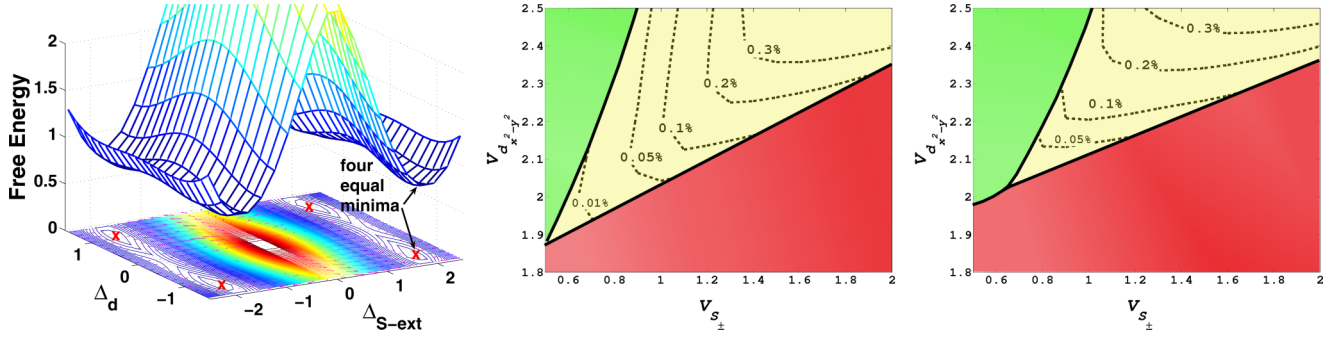


FIG. 5. (Color online) In (a) are shown free energy results as a function of the $d_{x^2-y^2}$ and S_{\pm} gaps ($\Delta_{d_{x^2-y^2}}$ and $\Delta_{S_{\pm}}$, respectively) exhibiting four degenerate total minima for which both order parameters are finite confirming the mixed nematic $S_{\pm} + d_{x^2-y^2}$ state. The dashed contour lines in (b) and (c) are equal free energy difference lines between the \mathcal{T} -violating SC phase and the nematic $S_{\pm} + d_{x^2-y^2}$ SC phase as a percentage of the free energy of the system in the $S_{\pm} + id_{x^2-y^2}$ state for $\mu = 0.05$ and $\mu = 0.4$, respectively. Note that the relative free energy difference for small values of the effective potentials is negligible and therefore nematic and \mathcal{T} -violating states are effectively degenerate.

APPENDIX B: NODAL VERSUS NODELESS SPECTRUM IN THE MIXED NEMATIC $S_{\pm} + d_{x^2-y^2}$ PHASE

In the nematic $S_{\pm} + d_{x^2-y^2}$ SC phase the quasiparticle energy spectrum becomes $E_{\lambda,l}^B(\mathbf{k}) = \lambda \sqrt{[\varepsilon_l(\mathbf{k})]^2 + [\Delta(\mathbf{k})]^2} - \mathcal{B}$ with $\lambda = \pm$, $l = e, h$, and $\Delta(\mathbf{k}) = \Delta_{S_{\pm}}(\cos k_x + \cos k_y) + \Delta_d(\cos k_x - \cos k_y)$. The l th band will have nodes when the conditions $\varepsilon_l(\mathbf{k}) = 0$ and $\Delta(\mathbf{k}) = 0$ are simultaneously satisfied. We consider here $|\mu| < 0.5$ and we obtain the following:

- (1) Nodes in both bands: $|\Delta_d| \geq \frac{10+4|\mu|}{2-4|\mu|} |\Delta_{S_{\pm}}|$.
- (2) Nodes only in the electron (hole) band for $\mu < 0$ ($\mu > 0$): $\frac{10+4|\mu|}{2-4|\mu|} |\Delta_{S_{\pm}}| > |\Delta_d| \geq \frac{10-4|\mu|}{2+4|\mu|} |\Delta_{S_{\pm}}|$.
- (3) Nodeless mixed $S_{\pm} + d_{x^2-y^2}$ SC phase: $\frac{10-4|\mu|}{2+4|\mu|} |\Delta_{S_{\pm}}| > |\Delta_d|$.

The coordinates of the nodes are shown to be defined from the equations $\cos k_x = \pm A/B_+$ and $\cos k_y = \pm A/B_-$ with $A = -2|\Delta_d| + \sqrt{(2\Delta_d)^2 + 2(2 \pm \mu)(\Delta_d^2 - \Delta_{S_{\pm}}^2)}$ and $B_{\pm} = |\Delta_{S_{\pm}} \pm \Delta_d|$. Here $+$ ($-$) give the nodes for the electron (hole) band. Two different equations for $\cos k_x$ and $\cos k_y$ reflect the symmetry reduction $C_4 \rightarrow C_2$ in the nematic $S_{\pm} + d_{x^2-y^2}$ SC phase. Our numerical results naturally verify the above and have led to the blue and green lines in the phase diagrams of Fig. 6.

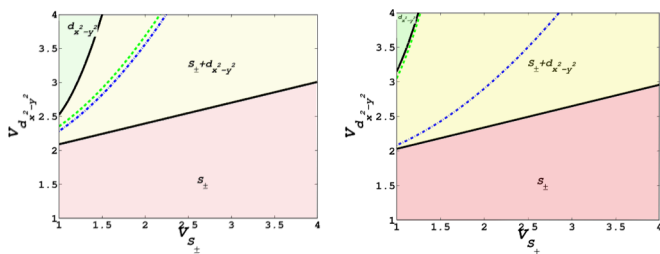


FIG. 6. (Color online) Phase diagram obtained with $T = \mathcal{B} = 0$ for (a) $\mu = 0.05$ and (b) $\mu = 0.4$. Solid line boundaries define the region over which the $S_{\pm} + d_{x^2-y^2}$ nematic phase is accessible. The green dashed line is the boundary above which the $S_{\pm} + d_{x^2-y^2}$ nematic SC phase exhibits nodes in both bands while the blue dash-dotted line is the boundary above which the $S_{\pm} + d_{x^2-y^2}$ nematic SC phase exhibits nodes only in the electron band for $\mu > 0$ or only in the hole band for $\mu < 0$.

APPENDIX C: INDUCED ELECTRONIC NEMATICITY EFFECTS COOPERATE WITH THE MIXED NEMATIC SUPERCONDUCTING PHASE AND STABILIZE IT

We can include the possibility of the formation of an electron nematic state by adding a term in the Hamiltonian that corresponds to a charge Pomeranchuk phase:

$$\mathcal{H} = \sum_{\mathbf{k}} \Psi_{\mathbf{k}}^{\dagger} \{ \gamma_{\mathbf{k}} \hat{\tau}_3 \hat{\rho}_0 + \delta_{\mathbf{k}} \hat{\tau}_3 \hat{\rho}_3 - \mu \hat{\tau}_3 \hat{\rho}_0 - \mathcal{B} \hat{\tau}_0 \hat{\rho}_0 + \Delta_{S_{\pm}}(\mathbf{k}) \hat{\tau}_1 \hat{\rho}_0 + \Delta_d(\mathbf{k}) \hat{\tau}_1 \hat{\rho}_0 + \mathcal{P}_{\mathbf{k}} \hat{\tau}_3 \hat{\rho}_0 \} \Psi_{\mathbf{k}}, \quad (\text{C1})$$

where $\mathcal{P}_{\mathbf{k}}$ corresponds to d -wave Pomeranchuk deformation: $\mathcal{P}_{\mathbf{k}} = \mathcal{P} f_{\mathbf{k}}^P$ and $f_{\mathbf{k}}^P = (\cos k_x - \cos k_y)$. We chose this specific Pomeranchuk state because $\mathcal{P}_{\mathbf{k}}$, $\Delta_{S_{\pm}}$, Δ_d , and $\gamma_{\mathbf{k}}$ form a quartet [44]. If a finite potential was present in this Pomeranchuk channel, we should have to study the mixed nematic superconducting state on the same footing with this charge Pomeranchuk order parameter adding an extra dimension in our phase maps. This demanding task will be attempted in a future work. However, even if we suppose that the potential in the Pomeranchuk channel is negligible, the emergence of a Pomeranchuk field induced by $\gamma_{\mathbf{k}}$, $\Delta_{S_{\pm}}$, and Δ_d lowers the free energy of the superconducting nematic state. The presence of a Pomeranchuk order parameter modifies the nearest-neighbor hopping matrix elements according to the corresponding symmetry breaking scheme $C_4 \rightarrow C_2$, yielding $t(\cos k_x + \cos k_y) \rightarrow t(\cos k_x + \cos k_y) - \mathcal{P}(\cos k_x - \cos k_y) = t(1 - \mathcal{P}/t) \cos k_x + t(1 + \mathcal{P}/t) \cos k_y$. Essentially, the initially isotropic nearest-neighbor hopping matrix element $t \equiv t_{x^2+y^2}$ decomposes into two nearest-neighbor hoppings: $t_{x^2} = t(1 - \mathcal{P}/t)$ and $t_{y^2} = t(1 + \mathcal{P}/t)$, which transform according to the trivial irreducible representation of the remaining point group symmetry after the $C_4 \rightarrow C_2$ symmetry breaking is effected. The presence of the nematic order parameter also affects the interactions that mediate the $S_{\pm} + d_{x^2-y^2}$ nematic superconductivity. Starting from the

effective interaction considered earlier,

$$\mathcal{V}_{\text{int}} = -\frac{1}{N} \sum_{\mathbf{k}, \mathbf{k}'} \widehat{\mathcal{D}}_{\mathbf{k}}^{\dagger} \begin{pmatrix} f_{s_{\pm}}(\mathbf{k}) & f_d(\mathbf{k}) \\ 0 & V_d \end{pmatrix} \begin{pmatrix} f_{s_{\pm}}(\mathbf{k}') \\ f_d(\mathbf{k}') \end{pmatrix} \widehat{\mathcal{D}}_{\mathbf{k}'}, \quad (\text{C2})$$

the irreducible representations entering the effective interaction above become modified in the following manner: $f_{s_{\pm}}^P(\mathbf{k}) = v_{x^2} \cos k_x + v_{y^2} \cos k_y$ and $f_d^P(\mathbf{k}) = v_{x^2} \cos k_x - v_{y^2} \cos k_y$, with $v_{x^2, y^2} = 1 \pm \eta P$ (with η an experimentally measurable coupling constant), providing

$$\mathcal{V}_{\text{int}} = -\frac{1}{N} \sum_{\mathbf{k}, \mathbf{k}'} \widehat{\mathcal{D}}_{\mathbf{k}}^{\dagger} \begin{pmatrix} f_{s_{\pm}}(\mathbf{k}) & f_d(\mathbf{k}) \\ \eta \mathcal{P}(V_{s_{\pm}} + V_d) & V_d \end{pmatrix} \begin{pmatrix} f_{s_{\pm}}(\mathbf{k}') \\ f_d(\mathbf{k}') \end{pmatrix} \widehat{\mathcal{D}}_{\mathbf{k}'}, \quad (\text{C3})$$

where we have kept only linear terms of η . The free energy functional assumes the form

$$\mathcal{F}_P = \frac{1}{2} \widehat{\Delta}^{\dagger} \begin{pmatrix} V_{s_{\pm}} & \eta \mathcal{P}(V_{s_{\pm}} + V_d) \\ \eta \mathcal{P}(V_{s_{\pm}} + V_d) & V_d \end{pmatrix}^{-1} \widehat{\Delta} + \frac{1}{2} \mathcal{P} T \sum_{\mathbf{k}, n} f_p(\mathbf{k}) \text{Tr}\{\hat{\tau}_3 \hat{\rho}_0 \hat{G}(\mathbf{k}, i\omega_n)\} - T \sum_{\mathbf{k}, n} \text{Tr}\{\ln \hat{G}^{-1}(\mathbf{k}, i\omega_n)\}, \quad (\text{C4})$$

where $\widehat{\Delta}^{\dagger} = (\Delta_{s_{\pm}}^*, \Delta_d^*)$ and $\mathcal{P} = T V_p \sum_{\mathbf{k}, n} f_p(\mathbf{k}) \text{Tr}\{\hat{\tau}_3 \hat{\rho}_0 \hat{G}(\mathbf{k}, i\omega_n)\} = V_p \mathcal{N}$. Extremizing the free energy with respect to the Pomeranchuk order parameter and taking the limit of zero potential in the Pomeranchuk channel we obtain the induced Pomeranchuk field,

$$P_{\text{ind}} = \left[\eta \left(\frac{1}{V_{s_{\pm}}} + \frac{1}{V_d} \right) (\Delta_{s_{\pm}}^* \Delta_d + \Delta_{s_{\pm}} \Delta_d^*) + T \sum_{\mathbf{k}, n} f_p(\mathbf{k}) \text{Tr}\{\hat{\tau}_3 \hat{\rho}_0 \hat{G}(\mathbf{k}, i\omega_n)|_{\mathcal{P}=0}\} \right] / \chi_P = \frac{\mathcal{N}_{\text{ind}}}{\chi_P}, \quad (\text{C5})$$

where $\chi_P = -T [f_p(\mathbf{k})]^2 \text{Tr}\{[\hat{\tau}_3 \hat{\rho}_0 \hat{G}_{\mathbf{k}}]^2\}$ is the Pomeranchuk susceptibility and \mathcal{N}_{ind} is the induced Pomeranchuk ordering. The change in free energy brought about by the additional ordering of the charge Pomeranchuk in the system is given by

$$\delta \mathcal{F}_P = \frac{1}{2} \widehat{\Delta}^{\dagger} \begin{pmatrix} 0 & \eta \mathcal{P}(V_{s_{\pm}} + V_d) \\ \eta \mathcal{P}(V_{s_{\pm}} + V_d) & 0 \end{pmatrix}^{-1} \widehat{\Delta} + T \frac{1}{2} \mathcal{P} \sum_{\mathbf{k}, n} f_p(\mathbf{k}) \text{Tr}\{\hat{\tau}_3 \hat{\rho}_0 \hat{G}(\mathbf{k}, i\omega_n)\} - T \sum_{\mathbf{k}} \text{Tr} \left\{ \ln \frac{\hat{G}^{-1}(\mathbf{k}, i\omega_n)}{\hat{G}^{-1}(\mathbf{k}, i\omega_n)|_{\mathcal{P}=0}} \right\}. \quad (\text{C6})$$

Assuming the induced Pomeranchuk ordering is sufficiently small we expand the above expression in \mathcal{P} up to second order

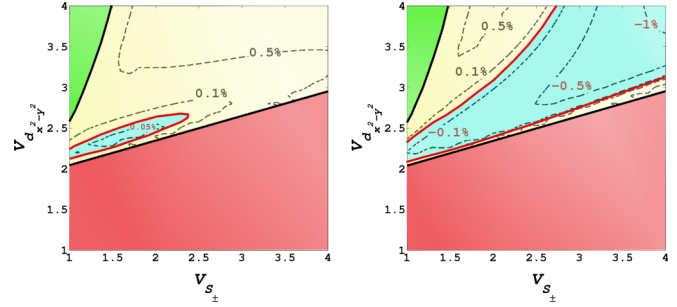


FIG. 7. (Color online) The relative free energy difference (dashed contour lines) between T -violating and nematic SC phases for $T = 0$, $\mu = 0.05$, and (a) $\eta = 0.055$, (b) $\eta = 0.08$. Note that modification of the interactions due to the induced Pomeranchuk field stabilizes the nematic SC phase over a wide range of the phase diagram (cyan area). Notice that for $\eta = 0.08$ the nematic SC phase is stabilized for potentials $V_{s_{\pm}} = V_d = 3$ corresponding to the tetracritical point case presented in the main text.

and again taking the limit of zero potential in the Pomeranchuk channel we obtain

$$\delta F_P = -P \frac{1}{2} \left[\eta \left(\frac{1}{V_{s_{\pm}}} + \frac{1}{V_d} \right) (\Delta_{s_{\pm}}^* \Delta_d + \Delta_{s_{\pm}} \Delta_d^*) + T \sum_{\mathbf{k}, n} f_p(\mathbf{k}) \text{Tr}\{\hat{\tau}_3 \hat{\rho}_0 \hat{G}(\mathbf{k}, i\omega_n)|_{\mathcal{P}=0}\} \right] = -\frac{[\mathcal{N}_{\text{ind}}]^2}{2\chi_P}, \quad (\text{C7})$$

where we have substituted the expression Eq. (C5) for the induced charge Pomeranchuk field. Utilizing Eq. (C7) we recalculated again the relative free energy difference between the nematic $S_{\pm} + d_{x^2-y^2}$ and the T -violating SC phase presented in Fig. 6 taking into account the free energy correction due to the induced charge Pomeranchuk field. For finite but small values of the coupling constant η the modification of the interaction lowers the free energy of the nematic $S_{\pm} + d_{x^2-y^2}$ phase enough in order to be stabilized with respect to the T -violating $S_{\pm} + id_{x^2-y^2}$ SC phase (Fig. 7).

APPENDIX D: A UNIFIED DESCRIPTION OF SHEAR AND ORTHORHOMBIC SUPERCONDUCTIVITY INDUCED NEMATICITY IN IRON-BASED SUPERCONDUCTORS

In the main discussion we have focused on nematic superconductivity originating from the $S_{\pm} + d_{x^2-y^2}$ SC phase which leads to an induced nematic order parameter with $f_{\text{nem}}(\mathbf{k}) = f_d(\mathbf{k})$ which corresponds to an orthorhombic distortion in the FBZ and a shear distortion in the BZ. In order to describe orthorhombic distortion in the BZ we have to study nematic superconductivity in the FBZ involving the d_{xy} superconducting order parameter instead of $d_{x^2-y^2}$ (see Fig. 8). Below we present some self-consistently extracted calculations for intraband superconducting pairing with identical gaps for both bands $\Delta(\mathbf{k})$ involving the irreducible representations $f_{s_{\pm}}(\mathbf{k}) = \cos k_x + \cos k_y$ and $f_d'(\mathbf{k}) = 2 \sin k_x \sin k_y$. In addition, within the Landau formalism and in the absence of nematic fluctuations, we find for S_{\pm} and d_{xy} the following: $|c - g|/\sqrt{\beta_1 \beta_2} = 0.23$ ($S_{\pm} + id_{xy}$ accessible) and

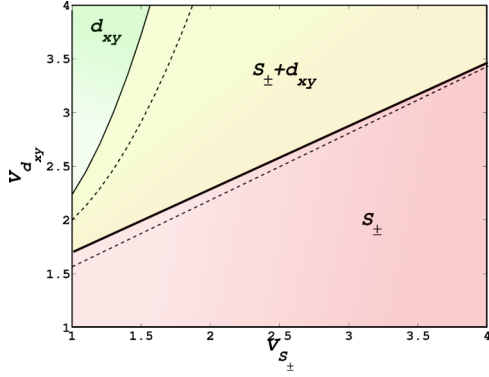


FIG. 8. (Color online) Phase diagram of the possible SC phases obtained by varying the effective interaction potentials of S_{\pm} and d_{xy} from t to $4t$ at $T = 0$. Solid line boundaries correspond to $\mu = 0.05$ and dashed line boundaries to $\mu = 0.4$. The extended region over which the two phases coexist corresponds to the nematic SC phase. The phase diagram is very similar to the corresponding diagram for S_{\pm} and $d_{x^2-y^2}$ presented in the main text; however in this case the chemical potential just shifts the nematic region to lower effective potentials of the d_{xy} phase.

$|c + g|/\sqrt{\beta_1\beta_2} = 0.69$ ($S_{\pm} + d_{xy}$ accessible). Furthermore, since $g > 0$ for this case, the \mathcal{T} -breaking phase will be favored in the absence of nematic fluctuations.

In the presence of nematic fluctuations, we have to include the appropriate correction to the free energy which can trip the balance towards a nematic phase. However, a complete investigation of the respective phase diagram including $f_{d'}(\mathbf{k})$ SC additionally requires the consideration of the $f_{s'}(\mathbf{k}) = 2 \cos k_x \cos k_y$ (A_1) SC order parameter. Since the order parameters Δ_s , $\Delta_{s_{\pm}}$, and $\Delta_{s'}$ belong to the same representation, bilinear couplings of the form $\Delta_m^* \Delta_n + \Delta_m \Delta_n^*$ with $n, m = \{s, s_{\pm}, s'\}$ are allowed, implying that all of these order parameters will be generally present if at least one of them is stabilized. The unavoidable presence of order parameters with the irreducible representation $f_{s'}(\mathbf{k})$ is crucial since the latter will become mixed with the $f_{d'}(\mathbf{k})$, relevant for shear nematicity in the FBZ. In this case, primarily the

combination $s' + d_{xy}$ induces shear nematicity in the FBZ and orthorhombic nematicity in the BZ. Consequently, in this extended model which will be presented in more detail elsewhere, both types of superconductivity induced nematicity are accessible in a unified description.

APPENDIX E: ANALOGY BETWEEN INTERBAND MIXED NEMATIC SPIN DENSITY WAVES AND MIXED NEMATIC SUPERCONDUCTIVITY

In this subsection, we demonstrate how the phase diagrams obtained in the main discussion concerning the coexistence and competition of intraband S_{\pm} and $d_{x^2-y^2}$ SCs suitably apply for mixed S_{\pm} and $d_{x^2-y^2}$ interband SDWs occurring from the nested electron and hole bands with wave vector $\mathbf{Q} = (\pi, \pi)$ in the folded Brillouin zone. For SDWs, we consider the following z -axis polarized interband allowed terms: $\sum_{\sigma} \sigma [M_{eh}(\mathbf{k})c_{k,\sigma}^{\dagger}d_{k+\mathbf{Q},\sigma} + M_{eh}^*(\mathbf{k})d_{k+\mathbf{Q},\sigma}^{\dagger}c_{k,\sigma}]$ and $\sum_{\sigma} \sigma [M_{he}(\mathbf{k})d_{k,\sigma}^{\dagger}c_{k+\mathbf{Q},\sigma} + M_{he}^*(\mathbf{k})c_{k+\mathbf{Q},\sigma}^{\dagger}d_{k,\sigma}]$. Since $\mathbf{Q} = (\pi, \pi)$ is commensurate, we obtain the important relation $M_{eh}(\mathbf{k} + \mathbf{Q}) = M_{he}^*(\mathbf{k})$. To describe the particular model microscopically we make use of the spinor $\widehat{\Psi}_{k,\sigma}^{\dagger} = (c_{k,\sigma}^{\dagger}, c_{k+\mathbf{Q},\sigma}^{\dagger}, d_{k,\sigma}^{\dagger}, d_{k+\mathbf{Q},\sigma}^{\dagger})$. The general Hamiltonian for the particular type of SDWs reads $\mathcal{H} = \sum_{k,\sigma} \widehat{\Psi}_{k,\sigma}^{\dagger} \widehat{\mathcal{H}}_{\sigma}(\mathbf{k}) \widehat{\Psi}_{k,\sigma}$ with

$$\begin{aligned} \widehat{\mathcal{H}}_{\sigma}(\mathbf{k}) = & \gamma(\mathbf{k})\hat{\kappa}_3 + \delta(\mathbf{k})\hat{\rho}_3 - \mu + \sigma [M_{\mathfrak{N},+}(\mathbf{k})\hat{\rho}_1\hat{\kappa}_1 \\ & - M_{\mathfrak{N},+}(\mathbf{k})\hat{\rho}_2\hat{\kappa}_1 - M_{\mathfrak{N},-}(\mathbf{k})\hat{\rho}_2\hat{\kappa}_2 - M_{\mathfrak{N},-}(\mathbf{k})\hat{\rho}_1\hat{\kappa}_2], \end{aligned} \quad (\text{E1})$$

where κ act on the $\mathbf{k}, \mathbf{k} + \mathbf{Q}$ space. The \pm index denotes the behavior of the order parameter under the translation $\mathbf{k} \rightarrow \mathbf{k} + \mathbf{Q}$. Notice that since $[\hat{\rho}_3, \gamma(\mathbf{k})\hat{\kappa}_3 + \delta(\mathbf{k})\hat{\rho}_3 - \mu] = 0$ we can arbitrarily choose the phase of the order parameters (when a single IR is present). Consequently the SDW order parameters behave as $U(1)$ order parameters in ρ -band space similar to the SC order parameters in τ -Nambu space. The only constraint imposed here, due to the commensurate nature of the nesting vector, is that order parameters even under translation $\mathbf{k} \rightarrow \mathbf{k} + \mathbf{Q}$ take the $\hat{\kappa}_1$ matrix, while the odd ones take the $\hat{\kappa}_2$ matrix. The energy spectrum reads

$$E_{\pm,+,\sigma}(\mathbf{k}) = -\mu \pm \sqrt{[\gamma(\mathbf{k}) + \delta(\mathbf{k})]^2 + [M_{\mathfrak{N},+}(\mathbf{k}) + M_{\mathfrak{N},-}(\mathbf{k})]^2 + [M_{\mathfrak{S},+}(\mathbf{k}) + M_{\mathfrak{S},-}(\mathbf{k})]^2}, \quad (\text{E2})$$

$$E_{\pm,-,\sigma}(\mathbf{k}) = -\mu \pm \sqrt{[\gamma(\mathbf{k}) - \delta(\mathbf{k})]^2 + [M_{\mathfrak{N},+}(\mathbf{k}) - M_{\mathfrak{N},-}(\mathbf{k})]^2 + [M_{\mathfrak{S},+}(\mathbf{k}) - M_{\mathfrak{S},-}(\mathbf{k})]^2}. \quad (\text{E3})$$

Note that there is a spin degeneracy. Below we write the spectra which determine the self-consistency equations and the related phase diagrams for both SDW and SC phases. We observe that if we set $\mu = 0$ in the SC case ($\mu_{sc} = 0$) and $\mathcal{B} = 0$ in the SDW case ($\mathcal{B}_{sdw} = 0$), there is a mapping between the SC and SDW phase diagrams by considering $\mu_{sdw} = \mathcal{B}_{sc}$.

$s_{\pm} + d$:

$$E_{\pm,\pm,\sigma}^{sdw}(\mathbf{k}) = -\mu \pm \sqrt{[\gamma(\mathbf{k}) \pm \delta(\mathbf{k})]^2 + [M_{s_{\pm}}(\mathbf{k}) + M_d(\mathbf{k})]^2}, \quad (\text{E4})$$

$$E_{\pm,\pm}^{sc}(\mathbf{k}) = -\mathcal{B} \pm \sqrt{[\gamma(\mathbf{k}) \pm \delta(\mathbf{k}) - \mu]^2 + [\Delta_{s_{\pm}}(\mathbf{k}) + \Delta_d(\mathbf{k})]^2}. \quad (\text{E5})$$

$s_{\pm} + id$:

$$E_{\pm,\pm,\sigma}^{sdw}(\mathbf{k}) = -\mu \pm \sqrt{[\gamma(\mathbf{k}) \pm \delta(\mathbf{k})]^2 + [M_{s_{\pm}}(\mathbf{k})]^2 + [M_d(\mathbf{k})]^2}, \quad (\text{E6})$$

$$E_{\pm, \pm}^{sc}(\mathbf{k}) = -\mathcal{B} \pm \sqrt{[\gamma(\mathbf{k}) \pm \delta(\mathbf{k}) - \mu]^2 + [\Delta_{s_{\pm}}(\mathbf{k})]^2 + [\Delta_d(\mathbf{k})]^2}. \quad (\text{E7})$$

It is straightforward that in the case of a zero field, exactly the same equations hold for a charge density wave (CDW) as well.

APPENDIX F: LANDAU EXPANSIONS OF THE FREE ENERGY IN A MIXED SUPERCONDUCTING STATE

1. Landau expansion when the SC order parameters have the same T_c

Starting from Eq. (A2), we can construct a Landau theory by expanding in terms of Δ_1 and Δ_2 the second term on the right-hand side. In what follows, we focus on the interplay between real s_{\pm} and $d_{x^2-y^2}$ SC order parameters (OPs), since it is their coexistence that leads to nematicity and sets $\mathcal{B} = 0$. The derivation of the Landau theory from our microscopic model allows us to systematically identify any possible anomalous coupling terms of linear or higher order that may acquire nonzero values, as well. After some algebra, and observing that both SC OPs share the same representation in this basis, the expression for the lowest-order cross-term is

$$\begin{aligned} \delta\mathcal{F}_1 &= \frac{1}{2}T \sum_{\mathbf{k}, n} \text{Tr}\{(\hat{\tau}_1 \hat{G}_0(\mathbf{k}, i\omega_n))^2\} \Delta_1(\mathbf{k}) \Delta_2(\mathbf{k}) \\ &= -\frac{1}{2} \sum_{\mathbf{k}, \pm} \frac{\Delta_1(\mathbf{k}) \Delta_2(\mathbf{k})}{\gamma_{\mathbf{k}} \pm \delta_{\mathbf{k}} - \mu} \tanh \frac{\gamma_{\mathbf{k}} \pm \delta_{\mathbf{k}} - \mu}{2T_c}. \end{aligned}$$

Clearly, whether this term is nonzero or not depends on the symmetry of the two SC OPs. For the specific case, the two form factors are orthogonal, since they correspond to different irreducible representations of the tetragonal point group, and the linear term identically vanishes.

Hence, the first coupling term that survives is the usual biquadratic (fourth order) term of the general form

$$\delta\mathcal{F}_2 = \frac{3}{4}T \sum_{\mathbf{k}, n} \text{Tr}\{(\hat{\tau}_1 \hat{G}_0(\mathbf{k}, i\omega_n))^4\} \Delta_1^2(\mathbf{k}) \Delta_2^2(\mathbf{k}).$$

This result explains why in all our self-consistent calculations we find $T_c^{s_{\pm}} \neq T_c^{d_{x^2-y^2}}$ except from the tetracritical point shown in Fig. 4(a).

We can write the effective free energy in the following form:

$$\begin{aligned} \mathcal{F}_{sc} &= \sum_{m=1,2} \left(\alpha_m \frac{|\Delta_m|^2}{2} + \beta_m \frac{|\Delta_m|^4}{4} \right) \\ &\quad + [c + g \cos(2\varphi)] \frac{|\Delta_1|^2 |\Delta_2|^2}{2}, \end{aligned} \quad (\text{F1})$$

where $\Delta_m = |\Delta_m| e^{i\varphi_m}$ and $\varphi = \varphi_1 - \varphi_2$. We obtain $\beta_m = S_{mm}$, $c = 2S_{12}$, and $g = S_{12} = c/2$ with

$$\begin{aligned} S_{ab} &= \frac{1}{N} \sum_{\mathbf{k}, l} \frac{[f_a(\mathbf{k}) f_b(\mathbf{k})]^2}{\varepsilon_l(\mathbf{k})} \frac{\partial}{\partial \varepsilon_l(\mathbf{k})} \\ &\quad \times \frac{n_F[\varepsilon_l(\mathbf{k}) - \mathcal{B}] - n_F[-\varepsilon_l(\mathbf{k}) - \mathcal{B}]}{2\varepsilon_l(\mathbf{k})} \Bigg|_{T=T_c}. \end{aligned} \quad (\text{F2})$$

(1) If $|c - g|/\sqrt{\beta_1 \beta_2} < 1$ the two order parameters can in principle coexist with $\varphi = \pi/2$, yielding a \mathcal{T} -violating phase with C_4 unbroken.

(2) If $|c + g|/\sqrt{\beta_1 \beta_2} < 1$ the two order parameters can in principle coexist with $\varphi = 0$ yielding a \mathcal{T} -invariant phase with $C_4 \rightarrow C_2$.

(3) If $g > 0$ ($g < 0$), the preferred coexistence phase is the \mathcal{T} -violating (C_4 -violating) phase.

With this expansion our findings can be summarized as follows:

(1) *For the pair of S and $d_{x^2-y^2}$* : For potentials $V_m \leq 4$, we find $0.4 \leq |c - g|/\sqrt{\beta_1 \beta_2} \leq 0.63$ ($S + id_{x^2-y^2}$ accessible) and $1 < |c + g|/\sqrt{\beta_1 \beta_2}$ ($S + d_{x^2-y^2}$ forbidden).

(2) *For the pair of S_{\pm} and $d_{x^2-y^2}$* : For potentials $2 \leq V_d \leq 4$ and $0.6 \leq V_{s_{\pm}} \leq 4$ we obtain $0.12 \leq |c - g|/\sqrt{\beta_1 \beta_2} < 0.33$ ($S_{\pm} + id_{x^2-y^2}$ accessible) and therefore $|c + g|/\sqrt{\beta_1 \beta_2} < 1$ ($S_{\pm} + d_{x^2-y^2}$ accessible) (Fig. 9).

2. Landau expansion when the SC OPs have different T_c

Similar results are obtained if we expand only about one of the OPs near its T_c , thus assuming $T_c^{s_{\pm}} \neq T_c^{d_{x^2-y^2}}$ from the beginning. The bilinear coupling term again averages to zero and the first finite-coupling term is the quadratic one: $\delta\mathcal{F}_2 = \frac{1}{4}T \sum_{\mathbf{k}, n} \text{Tr}\{[\hat{\tau}_1 \hat{G}_{\Delta_2=0}(\mathbf{k}, i\omega_n)]^2\} \Delta_2^2(\mathbf{k})$. Interestingly, the above term splits into two parts: the usual biquadratic term and another one that is a product between the square of the low T_c and a function of the higher T_c SC gap. Moreover, our calculations indicate that the conventional biquadratic term is in general positive, whereas the second term is negative. Thus, there can exist a point where the overall term becomes negative, leading to a coexisting phase between the two SC OPs at $T < T_{c_2} < T_{c_1}$.

We consider that the dominant order parameter is real ($\Delta_1 = |\Delta_1| \in \mathbb{R}$) and constant within the whole region where the subdominant ($\Delta_2 = |\Delta_2| e^{i\varphi}$) appears with a relative phase either $\varphi = 0$ (C_4 -violating) or $\varphi = \pi/2$ (\mathcal{T} -violating phase). Equivalently we can consider as independent variables the $\Delta_2^{\Re, \Im}$ (real, imaginary) components. The free energy expansion with respect to $\Delta_2^{\Re, \Im}$ assumes the following form:

$$\mathcal{F}_{sc} = \sum_{j=\Re, \Im} \left[\alpha_j \frac{(\Delta_2^j)^2}{2} + \beta_j \frac{(\Delta_2^j)^4}{4} \right] \quad (\text{F3})$$

with

$$\begin{aligned} \alpha_{\Re} &= \frac{2}{V_2} - \frac{1}{N} \sum_{\mathbf{k}, \lambda, l} \left[\frac{\Delta_1 f_1(\mathbf{k}) f_2(\mathbf{k})}{E_l^1(\mathbf{k})} \right]^2 \\ &\quad \times \left\{ \frac{\lambda n_F[E_{s, l}^{1, \mathcal{B}}(\mathbf{k})]}{E_l^1(\mathbf{k})} - n'_F[E_{\lambda, l}^{1, \mathcal{B}}(\mathbf{k})] \right\} \\ &\quad - \frac{[f_2(\mathbf{k})]^2 \lambda n_F[E_{\lambda, l}^{1, \mathcal{B}}(\mathbf{k})]}{E_l^1(\mathbf{k})}, \end{aligned} \quad (\text{F4})$$

$$\alpha_{\mathfrak{N}} = \frac{2}{V_2} + \frac{1}{N} \sum_{k,\lambda,l} \frac{[f_2(\mathbf{k})]^2 s n_F[E_{\lambda,l}^{1,B}(\mathbf{k})]}{E_l^1(\mathbf{k})}, \quad (\text{F5})$$

where $E_{\lambda,l}^{1,B}(\mathbf{k}) = \lambda \sqrt{[\varepsilon_l(\mathbf{k})]^2 + [\Delta_1(\mathbf{k})]^2} - \mathcal{B} = \lambda E_{\lambda,l}^1(\mathbf{k}) - \mathcal{B}$. We introduce the generalized susceptibilities $\chi_{\mathfrak{N},\mathfrak{S}} \equiv 1/V_2 - \alpha_{\mathfrak{N},\mathfrak{S}}/2$. As expected, for $\Delta_1 = 0$ the two expressions coincide. When $\Delta_1 \neq 0$ we can write $\chi_{\mathfrak{N}} = \chi_{\mathfrak{S}} + \delta\alpha/2$, with $\delta\alpha = \alpha_{\mathfrak{S}} - \alpha_{\mathfrak{N}}$. Note that $n'_F[E_{\lambda,l}^{1,B}(\mathbf{k})] < 0$ and $\sum_{\lambda} \lambda n_F[E_{\lambda,l}^{1,B}(\mathbf{k})] < 0 \forall k,l$. For $\delta\alpha > 0$ the critical temperature $T_{c,2}^{\mathfrak{N}}$ for the C_4 -violating SC phase is higher than the critical temperature $T_{c,2}^{\mathfrak{S}}$ for the \mathcal{T} -violating phase, stabilizing the former. In the opposite case $\delta\alpha < 0$ we obtain $T_{c,2}^{\mathfrak{N}} < T_{c,2}^{\mathfrak{S}}$ and the \mathcal{T} -violating phase becomes favored.

3. Stabilization of the nematic $S_{\pm} + d_{x^2-y^2}$ SC phase from an induced Pomeranchuk order parameter which only modifies the band structure

In the mixed $S_{\pm} + d_{x^2-y^2}$ nematic SC phase a $d_{x^2-y^2}$ nematic order parameter is spontaneously induced, which leads to a correction of the free energy. In order to calculate this correction, we need to infer the coupling between the nematic and SC order parameters. A nematic order parameter P which only modifies the band structure acts in the following way: $E_{\lambda,l}^{\mathfrak{S},\Phi}(\mathbf{k}) = \lambda \sqrt{[\varepsilon_l(\mathbf{k}) - \Phi f_d(\mathbf{k})]^2 + |\Delta_1(\mathbf{k}) + \Delta_2(\mathbf{k})|^2} - \mathcal{B}$, where we introduced the nematic field $\Phi = P/\chi_p$, with χ_p denoting the relevant nematic susceptibility. Once again we distinguish the cases:

(1) *Different critical temperatures* ($T_{c,1} \neq T_{c,2}$). The total free energy reads

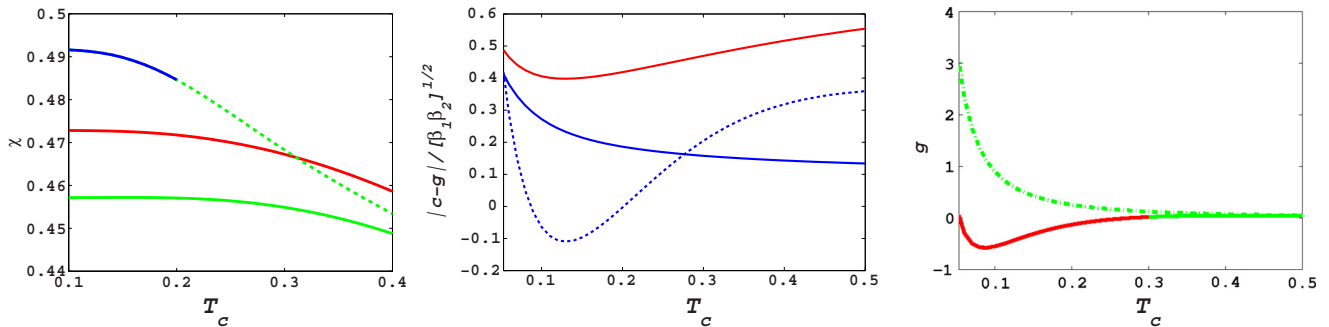


FIG. 9. (Color online) Left: The susceptibility for the $d_{x^2-y^2}$ SC phase emerging in $\varphi = 0$ (green solid line) and in $\varphi = \pi/2$ (red solid line) where the dominant order parameter is $\Delta_{S_{\pm}} = 0.5$. The green dashed line corresponds to the susceptibility $\tilde{\chi}_{\mathfrak{N}} = \chi_{\mathfrak{N}} + \frac{\psi_{BS}^2}{2\chi_p}$ including the correction due to the induction of a nematic order parameter modifying the band structure, when the nematic fluctuations are taken into account. The blue dash-dotted line corresponds to the susceptibility of $d_{x^2-y^2}$ SC phase for $\Delta_{S_{\pm}} = 0$. For $V_{S_{\pm}} = 1.45$ the critical temperature for the pure S_{\pm} phase is $T_c^{S_{\pm}} = 0.415$ and for $T < 0.2$ the order parameter acquires the value $\Delta_{S_{\pm}} = 0.5$ which remains constant until $T = 0$. For $V_d \simeq 2.06$ (which corresponds to a susceptibility $\tilde{\chi}_{\mathfrak{N}}^d \simeq 0.485$) the nematic $S_{\pm} + d_{x^2-y^2}$ will be stabilized at least near the $T_c^{\mathfrak{N}} \leq 0.2$ due to the presence of nematic fluctuations. Middle: The normalized $|c - g|/\sqrt{\beta_1 \beta_2}$ term for the $S + id_{x^2-y^2}$ (red line) and $S_{\pm} + id_{x^2-y^2}$ (blue line) with respect to the critical temperature T_c . The value remains always lower than 1 and therefore $S + id_{x^2-y^2}$ and $S_{\pm} + id_{x^2-y^2}$ are both accessible for potentials leading to common T_c . For $g > 0$ (which is always the case when nematic fluctuations are not considered) $|c + g|/\sqrt{\beta_1 \beta_2} = 3|c - g|/\sqrt{\beta_1 \beta_2}$. Therefore $S + d_{x^2-y^2}$ with common T_c is never accessible while $S_{\pm} + d_{x^2-y^2}$ is accessible for $1.97 \leq V_d \leq 4$ and $0.6 \leq V_{S_{\pm}} \leq 4$ yet not favored with respect to the \mathcal{T} -violating $S_{\pm} + id_{x^2-y^2}$ phase ($g > 0$). Even in the presence of nematic fluctuations the nematic $S_{\pm} + d_{x^2-y^2}$ phase is always accessible as $|\tilde{c} + \tilde{g}|/\sqrt{\beta_1 \beta_2} < 1$ (blue dashed line). Right: The term g for the S_{\pm} and $d_{x^2-y^2}$ with (solid green line) and without (dashed green line) considering nematic fluctuations. Including nematic fluctuations leads to $\tilde{g} < 0$ (red line) for common $0.05 < T_c < 0.28$ and nematic $S_{\pm} + d_{x^2-y^2}$ phase is favored with respect to the \mathcal{T} -violating $S_{\pm} + id_{x^2-y^2}$. In the range of potential $1.96 \leq V_d \leq 2.06$ and $0.65 \leq V_{S_{\pm}} \leq 1.19$ there is always a combination of potentials leading to common critical temperature $0.05 < T_c < 0.28$.

$$\mathcal{F}_{sc-nem} = \frac{P^2}{2\chi_p} + \sum_{j=\mathfrak{N},\mathfrak{S}} \left[\alpha_j \frac{(\Delta_2^j)^2}{2} + \beta_j \frac{(\Delta_2^j)^4}{4} \right] - \psi_{BS} \Delta_2^{\mathfrak{N}} \frac{P}{\chi_p}, \quad (\text{F6})$$

where the coupling ψ reads

$$\psi_{BS} = - \frac{\partial^2 \tilde{\mathcal{F}}_{sc}}{\partial \Delta_2^{\mathfrak{N}} \partial \Phi} \Big|_{\Delta_2^{\mathfrak{N}} = \Phi = 0} = \frac{\Delta_1}{N} \sum_{k,\lambda,l} \frac{\varepsilon_l(\mathbf{k}) f_2(\mathbf{k}) f_{nem}(\mathbf{k}) f_1(\mathbf{k})}{E_{k,1}^2} \times \left[n'_F[E_{\lambda,l}^{1,B}(\mathbf{k})] - \lambda \frac{n_F[E_{\lambda,l}^{1,B}(\mathbf{k})]}{E_{\lambda,l}^1(\mathbf{k})} \right], \quad (\text{F7})$$

where we have $\chi_p = -\partial^2 \mathcal{F}_{sc}/\partial \Phi^2$ calculated at $T = T_{c,2}$, $\Phi = 0$, and $\Delta_2 = 0$, yielding

$$\chi_p = -\frac{1}{N} \sum_{k,\lambda,l} f_p(\mathbf{k})^2 \left\{ \left[\frac{\varepsilon_l(\mathbf{k})}{E_l^1(\mathbf{k})} \right]^2 n'_F[E_{\lambda,l}^{1,B}(\mathbf{k})] + \lambda \left(\frac{\Delta_1(\mathbf{k})}{E_l^1(\mathbf{k})} \right)^2 \frac{n_F[E_{\lambda,l}^{1,B}(\mathbf{k})]}{E_l^1(\mathbf{k})} \right\}, \quad (\text{F8})$$

with $E_{\lambda,l}^{1,B}(\mathbf{k}) = \lambda \sqrt{[\varepsilon_l(\mathbf{k})]^2 + [\Delta_1(\mathbf{k})]^2} - \mathcal{B} = \lambda E_l^1(\mathbf{k}) - \mathcal{B}$. Extremization of the free energy with respect to the nematic order parameter provides $P_{ind}^{BS} = \psi_{BS} \Delta_2^R$ which leads to a renormalized free energy for superconductivity

$$\tilde{\mathcal{F}}_{sc} = \left(\alpha_{\mathfrak{N}} - \frac{\psi_{BS}^2}{\chi_p} \right) \frac{[\Delta_2^{\mathfrak{N}}]^2}{2} + \alpha_{\mathfrak{S}} \frac{(\Delta_2^{\mathfrak{S}})^2}{2} + \sum_{j=R,I} \beta_j \frac{(\Delta_2^j)^4}{4}. \quad (\text{F9})$$

The induced nematic order parameter effectively leads to an enhancement of the Δ_2^{nl} susceptibility and therefore to an increase of T_c^{nl} . If $\psi_{BS}^2/\chi_p > \delta\alpha$, the critical temperature of the nematic SC phase becomes higher than the critical temperature for the \mathcal{T} -violating phase, stabilizing the nematic. In Fig. 9 we present a particular case: according to our microscopic calculations the nematic fluctuations stabilize the nematic over the \mathcal{T} -violating phase.

(2) *The same critical temperature (T_c).* When $\Delta_{1,2}$ are both small in the vicinity of T_c we obtain

$$\begin{aligned} \mathcal{F}_{sc\text{-nem}} = & \frac{P^2}{2\chi_p} + \sum_{m=1,2} \left(\alpha_m \frac{|\Delta_m|^2}{2} + \beta_m \frac{|\Delta_m|^4}{4} \right) \\ & + [c + g \cos(2\varphi)] \frac{|\Delta_1|^2 |\Delta_2|^2}{2} \\ & - \psi_{BS} |\Delta_1| |\Delta_2| \frac{P}{\chi_p} \cos(\varphi), \end{aligned} \quad (\text{F10})$$

where in this case the nematic susceptibility reduces to the normal phase nematic susceptibility $\chi_p = -(1/N) \sum_{\mathbf{k}, \lambda, l} f_p(\mathbf{k})^2 \{n'_F[-\mathcal{B} + \lambda \varepsilon_l(\mathbf{k})]\}$ and the expression for the coupling constant ψ_{BS} in this case takes the form

$$\begin{aligned} \psi_{BS} = & - \left. \frac{\partial \mathcal{F}_{sc\text{-nem}}}{\partial (\Phi \Delta_1 \Delta_2^*)} \right|_{\Delta_1 = \Delta_2^* = \Phi = 0} \\ = & \frac{1}{N} \sum_{\mathbf{k}, \lambda, l} \frac{f_2(\mathbf{k}) f_{\text{nem}}(\mathbf{k}) f_1(\mathbf{k})}{\varepsilon_l(\mathbf{k})} \\ & \times \left[n'_F[-\mathcal{B} + \lambda \varepsilon_l(\mathbf{k})] - \lambda \frac{n_F[-\mathcal{B} + \lambda \varepsilon_l(\mathbf{k})]}{\varepsilon_l(\mathbf{k})} \right]. \end{aligned} \quad (\text{F11})$$

We obtain $P_{\text{ind}}^{BS} = \psi_{BS} |\Delta_1| |\Delta_2| \cos(\varphi)$ leading to the corrected free energy $\mathcal{F}_{sc\text{-nem}} = \sum_{m=1,2} (\alpha_m |\Delta_m|^2/2 + \beta_m |\Delta_m|^4/4) + [\tilde{c} + \tilde{g} \cos(2\varphi)] |\Delta_1|^2 |\Delta_2|^2/2$ with $\tilde{c} = c - \psi_{BS}^2/(2\chi_p)$ and $\tilde{g} = g - \psi_{BS}^2/(2\chi_p)$ where ψ_{BS} and χ_p are calculated for $T = T_c$. If $|\tilde{c} - \tilde{g}|/\sqrt{\beta_1 \beta_2} < 1$ the two order parameters can in principle coexist with $\varphi = \pi/2$, yielding a \mathcal{T} -violating phase with C_4 unbroken. Since $|\tilde{c} - \tilde{g}| = |c - g|$ the energy correction due to the presence of nematic fluctuations does not bring any modification here. If $|\tilde{c} + \tilde{g}|/\sqrt{\beta_1 \beta_2} = |c + g - \psi_{BS}^2/\chi_p|/\sqrt{\beta_1 \beta_2} < 1$ the two order parameters can in principle coexist with $\varphi = 0$ yielding a \mathcal{T} -invariant nematic phase. If $\tilde{g} > 0$ ($\tilde{g} < 0$) the preferred coexistence phase is the \mathcal{T} -violating (C_4 -violating) phase. In the presence of nematic fluctuations we find that the nematic phase is accessible and preferred compared to the \mathcal{T} breaking, only for an intermediate coupling (a similar result was found in Ref. [33]), since only in the latter case the conditions $\tilde{g} < 0$ and $|\tilde{c} + \tilde{g}|/\sqrt{\beta_1 \beta_2} < 1$ are simultaneously satisfied. Within our microscopic model we were able to identify the range of potentials for which the coupling ψ_{BS} is sufficient for the nematic $S_{\pm} + id_{x^2-y^2}$ SC phase to be accessible and also preferred with respect to the \mathcal{T} -violating phase (Fig. 9).

4. Stabilization of the nematic $S_{\pm} + d_{x^2-y^2}$ SC phase from an induced Pomeranchuk order parameter which modifies the band structure and the interaction potentials

In the most general case, a nematic field Φ and consequently a nematic order parameter P couple to the nematic SC phase via the nearest-neighbor hopping matrix elements according to the corresponding symmetry-breaking scheme $C_4 \rightarrow C_2$, yielding $t(\cos k_x + \cos k_y) \rightarrow t(\cos k_x + \cos k_y) - \Phi(\cos k_x - \cos k_y) = t(1 - \Phi/t) \cos k_x + t(1 + \Phi/t) \cos k_y$. Essentially, the initially isotropic nearest-neighbor hopping matrix element $t \equiv t_{x^2+y^2}$ decomposes into two nearest-neighbor hoppings: $t_{x^2} = t(1 - \Phi/t)$ and $t_{y^2} = t(1 + \Phi/t)$, which transform according to the trivial irreducible representation of the remaining point group symmetry after the $C_4 \rightarrow C_2$ symmetry breaking is effected. The presence of the nematic field also affects the interactions that mediate the $S_{\pm} + d_{x^2-y^2}$ nematic superconductivity (see also [33]). Starting from the effective interaction considered earlier $\mathcal{V}_{\text{int}} = -(1/N) \sum_{\mathbf{k}, \mathbf{k}'} \sum_{m=s_{\pm}, d} V_m f_m(\mathbf{k}) f_m(\mathbf{k}') \widehat{\mathcal{D}}_{\mathbf{k}}^{\dagger} \widehat{\mathcal{D}}_{\mathbf{k}'}$ the irreducible representations entering the effective interaction above become modified in the following manner: $f_{s_{\pm}}^{\Phi}(\mathbf{k}) = v_{x^2} \cos k_x + v_{y^2} \cos k_y$ and $f_d^{\Phi}(\mathbf{k}) = v_{x^2} \cos k_x - v_{y^2} \cos k_y$, with $v_{x^2, y^2} = 1 \pm \eta \Phi$ (with η an experimentally measurable coupling constant), providing

$$\begin{aligned} \mathcal{V}_{\text{int}} = & -\frac{1}{N} \sum_{\mathbf{k}, \mathbf{k}'} \widehat{\mathcal{D}}_{\mathbf{k}}^{\dagger} (f_{s_{\pm}}(\mathbf{k}) \quad f_d(\mathbf{k})) \\ & \times \begin{pmatrix} V_{s_{\pm}} + (\eta \Phi)^2 V_d & \eta \Phi (V_{s_{\pm}} + V_d) \\ \eta \Phi (V_{s_{\pm}} + V_d) & V_d + (\eta \Phi)^2 V_{s_{\pm}} \end{pmatrix} \begin{pmatrix} f_{s_{\pm}}(\mathbf{k}') \\ f_d(\mathbf{k}') \end{pmatrix} \widehat{\mathcal{D}}_{\mathbf{k}'}. \end{aligned} \quad (\text{F12})$$

By introducing the order parameters

$$\begin{aligned} \Delta_{s_{\pm}} = & -\frac{1}{N} \sum_{\mathbf{k}} \{ [V_{s_{\pm}} + (\eta \Phi)^2 V_d] f_{s_{\pm}}(\mathbf{k}) \\ & + \eta \Phi (V_{s_{\pm}} + V_d) f_d(\mathbf{k}) \} \widehat{\mathcal{D}}_{\mathbf{k}}, \end{aligned} \quad (\text{F13})$$

$$\begin{aligned} \Delta_d = & -\frac{1}{N} \sum_{\mathbf{k}} \{ [V_d + (\eta \Phi)^2 V_{s_{\pm}}] f_d(\mathbf{k}) \\ & + \eta \Phi (V_{s_{\pm}} + V_d) f_{s_{\pm}}(\mathbf{k}) \} \widehat{\mathcal{D}}_{\mathbf{k}}, \end{aligned} \quad (\text{F14})$$

we obtain the mean-field decoupled interaction $\mathcal{V}_{\text{int}} \simeq N \widehat{\Delta}^{\dagger} \widehat{\mathcal{V}}^{-1}(\Phi) \widehat{\Delta} + \sum_{\mathbf{k}} [\Delta(\mathbf{k}) \widehat{\mathcal{D}}_{\mathbf{k}}^{\dagger} + \text{H.c.}]$ with $\Delta(\mathbf{k}) = \Delta_{s_{\pm}} f_{s_{\pm}}(\mathbf{k}) + \Delta_d f_d(\mathbf{k})$, $\widehat{\Delta}^{\dagger} = (\Delta_{s_{\pm}}^* \Delta_d^*)$, and

$$\widehat{\mathcal{V}}(\Phi) = \begin{pmatrix} V_{s_{\pm}} + (\eta \Phi)^2 V_d & \eta \Phi (V_{s_{\pm}} + V_d) \\ \eta \Phi (V_{s_{\pm}} + V_d) & V_d + (\eta \Phi)^2 V_{s_{\pm}} \end{pmatrix}. \quad (\text{F15})$$

The free energy of the system $\tilde{\mathcal{F}}_{sc\text{-nem}}$ assumes then the form

$$\begin{aligned} \tilde{\mathcal{F}}_{sc\text{-nem}} = & \widehat{\Delta}^{\dagger} [\widehat{\mathcal{V}}^{-1}(\Phi) - \widehat{\mathcal{V}}^{-1}(0)] \widehat{\Delta} \\ & - \frac{1}{N\beta} \sum_{\mathbf{k}, \lambda, l} \ln[1 + e^{-\beta E_{\lambda, l}^{\text{B}, \Phi}(\mathbf{k})}], \end{aligned} \quad (\text{F16})$$

with $E_{\lambda, l}^{\text{B}, \Phi}(\mathbf{k}) = \lambda \sqrt{[\varepsilon_l(\mathbf{k}) + \Phi f_p(\mathbf{k})]^2 + |\Delta(\mathbf{k})|^2} - \mathcal{B}$. We distinguish the two cases:

(1) *Different critical temperatures* ($T_{c,1} \neq T_{c,2}$). Based on Eq. (F16) we obtain

$$\tilde{\mathcal{F}}_{sc-nem} = \frac{P^2}{2\tilde{\chi}_p} + \sum_{j=R,I} \left[\alpha_j \frac{(\Delta_2^j)^2}{2} + \beta_j \frac{(\Delta_2^j)^4}{4} \right] - \tilde{\psi} \Delta_2^{\text{Re}} \frac{P}{\tilde{\chi}_p}, \quad (\text{F17})$$

where only the nematic susceptibility and the coupling constant ψ acquire additional terms $\tilde{\chi}_p = \chi_p - \eta^2(2/V_1 + 1/V_2)\Delta_1^2 \simeq \chi_p$ [according to our approximation $\eta\Phi$ small, the diagonal correction term in the matrix of modified potentials Eq. (F15) is negligible] and $\tilde{\psi} = \psi_{BS} + 2\eta(1/V_1 + 1/V_2)\Delta_1$. We obtain the induced nematic order $P_{\text{ind}} = \tilde{\psi} \Delta_2^{\text{Re}}$ leading to $\tilde{\mathcal{F}}_{sc} = (\alpha_{\text{Re}} - \tilde{\psi}^2/\chi_p)(\Delta_2^{\text{Re}})^2/2 + \alpha_{\text{Im}}(\Delta_2^{\text{Im}})^2/2 + \sum_{j=R,I} \beta_j(\Delta_2^j)^4/4$.

(2) *The same critical temperature* (T_c). Starting from Eq. (F16) in the vicinity of T_c we obtain the additional contribution to the coupling constant ψ

$$\psi_V = 2\eta \left(\frac{1}{V_{\pm}} + \frac{1}{V_d} \right), \quad (\text{F18})$$

while the nematic susceptibility is not modified. Due to the inclusion of the additional contribution arising from the modified interactions we obtain $|\tilde{c}' + \tilde{g}'|/\sqrt{\beta_1\beta_2} = |c + g - (\psi + \psi_V)^2/\chi_p|/\sqrt{\beta_1\beta_2}$ and $\tilde{g}' = g - (\psi + \psi_V)^2/2\chi_p$ for the nematic $S_{\pm} + d_{x^2-y^2}$ phase. In the case in which the conditions $\tilde{g}' < 0$ and $|\tilde{c}' + \tilde{g}'|/\sqrt{\beta_1\beta_2} < 1$ are simultaneously satisfied, as mentioned in the previous paragraphs the nematic $S_{\pm} + d_{x^2-y^2}$ phase is accessible and also favored with respect to the \mathcal{T} -violating $S_{\pm} + id_{x^2-y^2}$ phase. Again for intermediate coupling and therefore small values of the coupling constant η , both conditions above are simultaneously satisfied and the nematic $S_{\pm} + id_{x^2-y^2}$ phase is stabilized at least at the vicinity of the critical temperature. We find that adding the contribution

to coupling ψ due to modified interaction, the nematic $S_{\pm} + id_{x^2-y^2}$ phase can be stabilized for a wider range of potentials. Particularly for $V_{\pm} = V_d = 3$ which corresponds to the case of the tetracritical point discussed in the main text, we find $\beta_{s_{\pm}} = 0.07$, $\beta_d = 0.057$, $c_{s_{\pm}-d} = 0.015$, and $\chi_p = 0.39$. For this case the coupling is between the superconducting and nematic order parameters without considering modification of interaction $\psi \simeq 0$, leading to $\tilde{g} > 0$, and the \mathcal{T} -violating phase is stabilized. Considering now that the induced nematic order parameter modifies interactions as described above, the coupling constant $\tilde{\psi} \simeq \psi_V$ acquires the necessary values for the nematic phase to be accessible $|\tilde{c}' + \tilde{g}'|/\sqrt{\beta_1\beta_2} < 1$ and preferred $\tilde{g}' < 0$ for $0.057 < |\eta| < 0.127$.

Since the coupling constant η is crucial for determining the phase diagram which is realizable in the iron-based superconductors, it is necessary to retrieve experimentally the value of η introduced in the previous paragraph. For $\eta \neq 0$ the effect of a nematic field Φ is to enhance the critical temperature [33]. The modified equation that provides the critical temperature is given from the zeros of the determinant

$$\begin{vmatrix} (V_{s_{\pm}} + (\eta\Phi)^2 V_d & \eta\Phi(V_{s_{\pm}} + V_d))^{-1} & \begin{pmatrix} \chi_{s_{\pm}} & 0 \\ 0 & \chi_d \end{pmatrix} \\ \eta\Phi(V_{s_{\pm}} + V_d) & V_d + (\eta\Phi)^2 V_{s_{\pm}} \end{vmatrix} = 0, \quad (\text{F19})$$

where we have introduced the susceptibilities

$$\chi_m = \frac{1}{N} \sum_{\mathbf{k},l} [f_m(\mathbf{k})]^2 \frac{n_F[-\varepsilon_l(\mathbf{k}) - \mathcal{B}] - n_F[\varepsilon_l(\mathbf{k}) - \mathcal{B}]}{2\varepsilon_l(\mathbf{k})}, \quad (\text{F20})$$

with $m = s_{\pm}, d$. If we assume that we apply orthorhombic strain in the FBZ then Φ will become finite and can be determined through the resistivity anisotropy $\rho_{xx} - \rho_{yy}$. For known Φ and the difference $T_c^{\Phi} - T_c^0$ in the presence and absence of strain, one can retrieve η from the equation above.

[1] H. Ding, P. Richard, K. Nakayama, K. Sugawara, T. Arakane, Y. Sekiba, A. Takayama, S. Souma, T. Sato, T. Takahashi, Z. Wang, X. Dai, Z. Fang, G. F. Chen, J. L. Luo, and N. L. Wang, *Europhys. Lett.* **83**, 47001 (2008); K. Terashima, Y. Sekiba, J. H. Bowen, K. Nakayama, T. Sato, P. Richard, Y.-M. Xu, L. J. Li, G. H. Cao, Z.-A. Xu, H. Ding, and T. Takahashi, *Proc. Natl. Acad. Sci. USA* **106**, 7330 (2009); Y. Zhang, L. X. Yang, M. Xu, Z. R. Ye, F. Chen, C. He, H. C. Xu, J. Jiang, B. P. Xie, J. J. Ying, X. F. Wang, X. H. Chen, J. P. Hu, M. Matsunami, S. Kimura, and D. L. Feng, *Nat. Mater.* **10**, 273 (2011).

[2] I. I. Mazin, D. J. Singh, M. D. Johannes, and M. H. Du, *Phys. Rev. Lett.* **101**, 057003 (2008); V. Stanev, J. Kang, and Z. Tesanovic, *Phys. Rev. B* **78**, 184509 (2008); A. V. Chubukov, D. V. Efremov, and I. Eremin, *ibid.* **78**, 134512 (2008).

[3] J. D. Fletcher, A. Serafin, L. Malone, J. G. Analytis, J.-H. Chu, A. S. Erickson, I. R. Fisher, and A. Carrington, *Phys. Rev. Lett.* **102**, 147001 (2009); J. K. Dong, S. Y. Zhou, T. Y. Guan, H. Zhang, Y. F. Dai, X. Qiu, X. F. Wang, Y. He, X. H. Chen, and S. Y. Li, *ibid.* **104**, 087005 (2010); Y. Nakai, T. Iye, S. Kitagawa, K. Ishida, S. Kasahara, T. Shibauchi, Y. Matsuda, and T. Terashima,

Phys. Rev. B **81**, 020503 (2010); M. Yamashita, Y. Senshu, T. Shibauchi, S. Kasahara, K. Hashimoto, D. Watanabe, H. Ikeda, T. Terashima, I. Vekhter, A. B. Vorontsov, and Y. Matsuda, *ibid.* **84**, 060507(R) (2011); Y. Zhang, Z. R. Ye, Q. Q. Ge, F. Chen, Juan Jiang, M. Xu, B. P. Xie, and D. L. Feng, *Nat. Phys.* **8**, 371 (2012); X. Qiu, S. Y. Zhou, H. Zhang, B. Y. Pan, X. C. Hong, Y. F. Dai, Man Jin Eom, Jun Sung Kim, Z. R. Ye, Y. Zhang, D. L. Feng, and S. Y. Li, *Phys. Rev. X* **2**, 011010 (2012).

[4] A. Aperis, P. Kotetes, G. Varelogiannis, and P. M. Oppeneer, *Phys. Rev. B* **83**, 092505 (2011).

[5] A. Aperis and G. Varelogiannis, *arXiv:1303.2231*.

[6] R. Thomale, C. Platt, W. Hanke, and B. A. Bernevig, *Phys. Rev. Lett.* **106**, 187003 (2011); R. Thomale, C. Platt, W. Hanke, J. Hu, and B. A. Bernevig, *ibid.* **107**, 117001 (2011).

[7] S. Maiti, M. M. Korshunov, T. A. Maier, P. J. Hirschfeld, and A. V. Chubukov, *Phys. Rev. B* **84**, 224505 (2011).

[8] R. M. Fernandes and A. J. Millis, *Phys. Rev. Lett.* **110**, 117004 (2013).

[9] G. Varelogiannis, *Phys. Rev. B* **57**, 13743 (1998); P. M. Oppeneer and G. Varelogiannis, *ibid.* **68**, 214512 (2003).

- [10] T. Hanke, S. Sykora, R. Schlegel, D. Baumann, L. Harnagea, S. Wurmehl, M. Daghofer, B. Buchner, J. van den Brink, and C. Hess, *Phys. Rev. Lett.* **108**, 127001 (2012).
- [11] J. J. Lee, F. T. Schmitt, R. G. Moore, S. Johnston, Y.-T. Cui, W. Li, M. Yi, Z. K. Liu, M. Hashimoto, Y. Zhang, D. H. Lu, T. P. Devereaux, D.-H. Lee, and Z.-X. Shen, *Nature (London)* **515**, 245 (2014).
- [12] Fong-Chi Hsu, Jiu-Yong Luo, Kuo-Wei Yeh, Ta-Kun Chen, Tzu-Wen Huang, P. M. Wu, Yong-Chi Lee, Yi-Lin Huang, Yan-Yi Chu, Der-Chung Yan, and Maw-Kuen Wu, *Proc. Natl. Acad. Sci. USA* **105**, 14262 (2008).
- [13] Y. Mizuguchi and Y. Takano, *J. Phys. Soc. Jpn.* **79**, 102001 (2010).
- [14] R. Khasanov, M. Bendele, K. Conder, H. Keller, E. Pomjakushina, and V. Pomjakushin, *New J. Phys.* **12**, 073024 (2010).
- [15] Can-Li Song, Yi-Lin Wang, Peng Cheng, Ye-Ping Jiang, Wei Li, Tong Zhang, Zhi Li, Ke He, Lili Wang, Jin-Feng Jia, Hsiang-Hsuan Hung, Congjun Wu, Xucun Ma, Xi Chen, and Qi-Kun Xue, *Science* **332**, 1410 (2011).
- [16] E. Fradkin, S. A. Kivelson, M. J. Lawler, J. P. Eisenstein, and A. P. Mackenzie, *Annu. Rev. Condens. Matter Phys.* **1**, 153 (2010); A. V. Chubukov, R. M. Fernandes, and J. Schmalian, *Nat. Phys.* **10**, 97 (2014).
- [17] S. Kasahara, H. J. Shi, K. Hashimoto, S. Tonegawa, Y. Mizukami, T. Shibauchi, K. Sugimoto, T. Fukuda, T. Terashima, Andriy H. Nevidomskyy, and Y. Matsuda, *Nature (London)* **486**, 382 (2012).
- [18] J.-H. Chu, H.-H. Kuo, J. G. Analytis, and I. R. Fisher, *Science* **337**, 710 (2012).
- [19] Ch. Meingast, F. Hardy, R. Heid, P. Adelmann, A. Bohmer, P. Burger, D. Ernst, R. Fromknecht, P. Schweiss, and T. Wolf, *Phys. Rev. Lett.* **108**, 177004 (2012).
- [20] A. E. Böhmer, P. Burger, F. Hardy, T. Wolf, P. Schweiss, R. Fromknecht, H. v. Löhneysen, C. Meingast, H. K. Mak, R. Lortz, S. Kasahara, T. Terashima, T. Shibauchi, and Y. Matsuda, *Phys. Rev. B* **86**, 094521 (2012).
- [21] C. Fang, H. Yao, W.-F. Tsai, J. Hu, and S. A. Kivelson, *Phys. Rev. B* **77**, 224509 (2008); J. Hu, C. Setty, and S. A. Kivelson, *ibid.* **85**, 100507(R) (2012).
- [22] C. Xu, M. Müller, and S. Sachdev, *Phys. Rev. B* **78**, 020501(R) (2008); E.-G. Moon and S. Sachdev, *ibid.* **85**, 184511 (2012).
- [23] Q. Si and E. Abrahams, *Phys. Rev. Lett.* **101**, 076401 (2008); P. Goswami, R. Yu, Q. Si, and E. Abrahams, *Phys. Rev. B* **84**, 155108 (2011).
- [24] R. M. Fernandes, L. H. VanBebber, S. Bhattacharya, P. Chandra, V. Keppens, D. Mandrus, M. A. McGuire, B. C. Sales, A. S. Sefat, and J. Schmalian, *Phys. Rev. Lett.* **105**, 157003 (2010); R. M. Fernandes, A. V. Chubukov, J. Knolle, I. Eremin, and J. Schmalian, *Phys. Rev. B* **85**, 024534 (2012).
- [25] T. M. McQueen, A. J. Williams, P. W. Stephens, J. Tao, Y. Zhu, V. Ksenofontov, F. Casper, C. Felser, and R. J. Cava, *Phys. Rev. Lett.* **103**, 057002 (2009).
- [26] W. Lv and P. Phillips, *Phys. Rev. B* **84**, 174512 (2011).
- [27] V. Stanev and P. B. Littlewood, *Phys. Rev. B* **87**, 161122 (2013).
- [28] Hsiang-Hsuan Hung, Can-Li Song, Xi Chen, Xucun Ma, Qi-kun Xue, and Congjun Wu, *Phys. Rev. B* **85**, 104510 (2012).
- [29] T. Shimojima, Y. Suzuki, T. Sonobe, A. Nakamura, M. Sakano, J. Omachi, K. Yoshioka, M. Kuwata-Gonokami, K. Ono, H. Kumigashira, A. E. Bohmer, F. Hardy, T. Wolf, C. Meingast, H. v. Löhneysen, H. Ikeda, and K. Ishizaka, *Phys. Rev. B* **90**, 121111(R) (2014); S.-H. Baek, D. V. Efremov, J. M. Ok, J. S. Kim, J. van den Brink, and B. Buchner, *Nat. Mater.* **14**, 210 (2015); A. E. Böhmer, T. Arai, F. Hardy, T. Hattori, T. Iye, T. Wolf, H. v. Löhneysen, K. Ishida, and C. Meingast, *arXiv:1407.5497*.
- [30] H. Kotegawa, S. Masaki, Y. Awai, H. Tou, Y. Mizuguchi, and Y. Takan, *J. Phys. Soc. Jpn.* **77**, 113703 (2008).
- [31] J. K. Dong, T. Y. Guan, S. Y. Zhou, X. Qiu, L. Ding, C. Zhang, U. Patel, Z. L. Xiao, and S. Y. Li, *Phys. Rev. B* **80**, 024518 (2009).
- [32] J.-Y. Lin, Y. S. Hsieh, D. A. Chareev, A. N. Vasiliev, Y. Parsons, and H. D. Yang, *Phys. Rev. B* **84**, 220507(R) (2011).
- [33] R. M. Fernandes and A. J. Millis, *Phys. Rev. Lett.* **111**, 127001 (2013).
- [34] M. H. S. Amin, S. N. Rashkeev, M. Coury, A. N. Omelyanchouk, and A. M. Zagoskin, *Phys. Rev. B* **66**, 174515 (2002).
- [35] P. Fulde, *Adv. Phys.* **22**, 667 (1973).
- [36] M. Sigrist and K. Ueda, *Rev. Mod. Phys.* **63**, 239 (1991); R. Joynt and L. Taillefer, *ibid.* **74**, 235 (2002).
- [37] A. B. Vorontsov, M. G. Vavilov, and A. V. Chubukov, *Phys. Rev. B* **81**, 174538 (2010).
- [38] M. Daghofer, A. Nicholson, A. Moreo, and E. Dagotto, *Phys. Rev. B* **81**, 014511 (2010).
- [39] S. Maiti and A. V. Chubukov, *Phys. Rev. B* **87**, 144511 (2013).
- [40] R. M. Fernandes and J. Schmalian, *Phys. Rev. B* **84**, 012505 (2011); V. Stanev, B. S. Alexandrov, P. Nikolic, and Z. Tesanovic, *ibid.* **84**, 014505 (2011); B. Mazidian, J. Quintanilla, A. D. Hillier, and J. F. Annett, *ibid.* **88**, 224504 (2013).
- [41] G. Varelogiannis, *Phys. Rev. Lett.* **88**, 117005 (2002).
- [42] C. Platt, R. Thomale, C. Honerkamp, S.-C. Zhang, and W. Hanke, *Phys. Rev. B* **85**, 180502 (2012).
- [43] G. Varelogiannis, *Phys. Rev. Lett.* **85**, 4172 (2000).
- [44] G. Varelogiannis, *arXiv:1305.2976*.
- [45] S. Chakravarty, R. B. Laughlin, D. K. Morr, and C. Nayak, *Phys. Rev. B* **63**, 094503 (2001).
- [46] J.-X. Zhu and A. V. Balatsky, *Phys. Rev. B* **65**, 132502 (2002); P. Kotetes and G. Varelogiannis, *ibid.* **80**, 212401 (2009).
- [47] S. Tewari, C. Zhang, V. M. Yakovenko, and S. Das Sarma, *Phys. Rev. Lett.* **100**, 217004 (2008); P. Kotetes and G. Varelogiannis, *Phys. Rev. B* **78**, 220509(R) (2008); *Europhys. Lett.* **84**, 37012 (2008); C.-H. Hsu, S. Raghu, and S. Chakravarty, *Phys. Rev. B* **84**, 155111 (2011).
- [48] P. Kotetes and G. Varelogiannis, *Phys. Rev. Lett.* **104**, 106404 (2010).
- [49] Y. Wang, Lu Li, and N. P. Ong, *Phys. Rev. B* **73**, 024510 (2006).
- [50] A. Kondrat, G. Behr, B. Büchner, and C. Hess, *Phys. Rev. B* **83**, 092507 (2011).